MINISTRY OF HIGHER EDUCATION AND SCIENTIFIC RESEARCH

UNIVERSITY FELIX HOUPHOUET BOIGNY

TRAINING AND RESEARCH UNIT FOR STRUCTURE SCIENCES OF MATTER AND TECHNOLOGY

REBUBLIC OF CÔTE D'IVORE
UNION-DISCIPLINE-TRAVAIL

DEPARTMENT OF PROCESS METALLURGY AND METAL RECYCLING OF RWTH AACHEN UNIVERSITY

SPONSORED BY THE

Federal Ministry of Education and Research

N°: 828

INTERNATIONAL MASTER PROGRAM

IN RENEWABLE ENERGY AND GREEN HYDROGEN

SPECIALITY: PRODUCTION AND TECHNOLOGY OF GREEN HYDROGEN

MASTER THESIS

Topic:

ADVANCES IN UNDERSTANDING OF DIRECT REDUCTION USING HYDROGEN

Presented on September 24, 2025, by:

Abdul Majid IS-HAK

JURY:

Prof. Kouadio Kouassi Yves	**President**	**Full Professor UFHB**
Prof. Ello Aimé Serge	**Examiner**	**Full Professor UFHB**
Dr. Fassinou W. Ferdinand	**Main Supervisor**	**Associate Professor UFHB**
Dr. -Ing. Srećko Stopić	**Co-Supervisor**	**Associate Professor RWTH-AU**

ACADEMIC YEAR 2024-2025

DEDICATION

I dedicate this write up to my late father, Mr. Is-hak Yussif. May The Almighty Allah have mercy on his gentle soul, to my mother, Hajia Fulera Issah for her immense support throughout my life and to the gallant heroes who lost their precious lives in the tragic helicopter crash in Ghana on August 6, 2025.

ACKNOWLEDGEMENT

All thanks and praise to Almighty Allah for His sustenance and for seeing me through this successful journey. I am highly indebted to WASCAL and BMBF (Federal Ministry of Education and Research in Germany) for their worthy cause of supporting West African youth through the International Masters Programme in Energy and Green Hydrogen Scholarship. I would like to say thank you to the Chancellor of Felix Houphouet Boigny University, Professor Ballo Zié for making it possible to continue the second year of this master's programme in Cote d'Ivoire. A big thank you also goes to both the Chancellor of the University of Lome, Togo and Abdou Moumouni University, Niger, Professor Adama Mawulé Kpodar Saidou and Professor Moussa Baragé respectively for hosting the first year (first and second semesters) of this master's programme.

My heartfelt gratitude goes to Professor Bernd Friedrich, the director of IME at RWTH Aachen University, Germany, for granting me access to the institute's laboratory and other facilities during my research stay in Germany. Special thanks go to Professor Rabbani Adamou, the director of WASCAL in Abdou Moumouni University, Niger for his unwavering support and guidance throughout the master's programme. I would also like to appreciate Professor Edouard Kouassi and Professor Ngolo Kone, the director and deputy director of WASCAL in Cote d'Ivoire respectively for all the support during the second year of the master's programme. To Professor Wanignon Ferdinand Fassinou, the coordinator of the Green Hydrogen Programme in Cote d'Ivoire who doubles up as my main supervisor for his guidance and advise in shaping this piece of work from its inception to the end. I also extend a heartfelt gratitude to my abled co-supervisor, Dr. Srećko Stopić for his continued guidance, support and direction. To the experienced jury members, presided by Professor Kouadio Kouassi Yves with Professor Ello Aimé Serge, the examiner, who helped in evaluating this piece of work, I am grateful for your invaluable comments and contributions.

This acknowledgement would be incomplete without the mention of Mr. Hanwen Chung of IME, RWTH University in Germany. I say thank you for your daily supervision and guidance throughout this piece of work. Finally, I would like to say a big thank you to all my family and friends who in one way or the other contributed to bringing this work to a successful end.

ABSTRACT

The hydrogen reduction of metal oxides presents a suitable substitute to traditional carbon-based reduction due to obvious reasons of eliminating carbon emissions. In this study, the advances in the understanding of the hydrogen reduction of a metal oxide, namely tellurium oxide, was investigated to determine the mechanism of the reaction. The investigation employed modelled and model free kinetic analysis of DTA-TG data of tellurium oxide under a hydrogen atmosphere at various heating rates. Further exploration of the process involved trial experiments in an oscillating kiln device at varying mass, time and temperature. Results from the study reveal a possible fit of the reduction process in more than one reaction model, indicating a multi-mechanistic reduction process. It was concluded from the kinetic analysis that the process could be a sequential or simultaneous overlapping of different rate limiting steps featuring diffusion, surface reaction and nucleation and growth of metal crystals. Reduction rates of the reduction process estimated from experimental trials demonstrate that the reaction is possible below the melting point of tellurium. Reduction rates of up to 100 % were achieved for experimental temperature of 600 ºC at different dwelling times. The experimental results also show that temperature variation significantly influences the reduction rate than variation in dwelling time and mass do. The study and its findings form part of the early explorations of the hydrogen reduction of tellurium oxide for future reference and comparison. Future studies should therefore verify the individual reaction regimes of the entire multi-step process suggested in the proposed reaction mechanism of the reduction process.

Keywords: Hydrogen reduction; tellurium; tellurium oxide; kinetic analysis; solid-gas reaction.

RESUME

La réduction des oxydes métalliques par l'hydrogène constitue une alternative intéressante à la réduction traditionnelle basée sur le carbone, notamment pour des raisons évidentes d'élimination des émissions de carbone. Dans cette étude, les avancées dans la compréhension de la réduction par l'hydrogène d'un oxyde métallique, l'oxyde de tellure, ont été étudiées afin de déterminer le mécanisme de la réaction. L'étude a utilisé une analyse cinétique modélisée et sans modèle des données DTA-TG de l'oxyde de tellure sous atmosphère d'hydrogène à différentes vitesses de chauffage. Une exploration plus approfondie du processus a impliqué des essais dans un four oscillant à masse, durée et température variables. Les résultats de l'étude révèlent une possible adéquation du processus de réduction à plusieurs modèles réactionnels, indiquant un processus de réduction multi-mécanique. L'analyse cinétique a conclu que le processus pourrait être une superposition séquentielle ou simultanée de différentes étapes limitantes de vitesse, comprenant la diffusion, la réaction de surface, la nucléation et la croissance de cristaux métalliques. Les taux de réduction du processus de réduction, estimés à partir d'essais expérimentaux, démontrent que la réaction est possible en dessous du point de fusion du tellure. Des taux de réduction allant jusqu'à 100 % ont été obtenus pour une température expérimentale de 600 °C à différents temps de séjour. Les résultats expérimentaux montrent également que les variations de température influencent significativement le taux de réduction, plus que les variations du temps de séjour et de la masse. Cette étude et ses résultats s'inscrivent dans les premières explorations de la réduction de l'oxyde de tellure par l'hydrogène, à des fins de référence et de comparaison ultérieures. Les études futures devraient donc vérifier les régimes réactionnels individuels de l'ensemble du processus multi-étapes suggéré dans le mécanisme réactionnel proposé pour le processus de réduction.

Mots-clés : Réduction de l'hydrogène ; tellure ; oxyde de tellure ; analyse cinétique ; réaction solide-gaz.

TABLE OF CONTENT

LIST OF FIGURES

LIST OF TABLES

ACRONYMS AND ABBREVIATIONS

3D: Three Dimensional

CD: Compact Disc

CdTe: Cadmium-telluride

COURSE50: CO_2 Ultimate Reduction System by innovative technology for cool Earth 50

DFT: Density Function Theory

DTA: Differential Thermal Analysis

DVD: Digital Video Disc

EDS: Energy Dispersive Spectroscopy

FTEL: First Tellurium Corporation

HARARE: Hydrogen As Reducing Agent in Recovery of metals and minerals from metallurgical waste.

HYBRIT: Hydrogen Breakthrough Ironmaking Technology

ICP-OES: Inductively Coupled Plasma - Optical Emissions

IME: Institute of Process Metallurgy and Metal Recycling

JMAK: Johnson Mehl Avrami Kolmogorov

PCM: Phase Change Memory

ppm: part per million

PV: Photovoltaic

RSC: Royal Society of Chemistry

RWTH: Rheinish-Westphalian Technical University

SALCOS: Salzgitter Low CO_2 Steelmaking

SEM: Scanning Electron Microscopy

TGA: Thermogravimetric Analysis

XRD: X-Ray Diffraction

GENERAL INTRODUCTION

INTRODUCTION

The need for sustainable energy in today's world has become indispensable. This need has sparked various innovations in the energy sector and has seen an immense growth in the provision of sustainable energy solutions. From the generation of energy through advanced renewable energy technologies to the manufacture of state-of-the-art energy storage and recovery systems, aiming at minimizing carbon footprints, promoting access to clean energy, increasing energy efficiency and in the long run, eradicating the escalating impacts of climate change. Tellurium, a time and again neglected and scarce element, is taking on a pivotal role in advancing innovations with respect to sustainable energy solutions (FTEL, 2023). The metalloid is believed to be influential in transforming the renewable energy field and can contribute to the realization of a greener, sound and sustainable energy in the future. Tellurium retains distinctive properties that make it exceptionally useful not only in the energy sector but in various industrial applications. For instance, in metallurgy, tellurium has various applications in metals such as steel, copper, lead and iron where it can serve as an accompaniment or alloying agent for free engineering, can be used to improve fatigue and opposition to vibrations, assist in minimizing the extent of chill and can act as a stabilizer in metals (Chivers & Laitinen, 2015; Rombach & Friedrich, 2014). In the field of electronics and energy, the suboxide of the metal is used in memory chips and discs (CD, DVD) and semi-conducting metal tellurides are used for various applications such as thermoelectric materials in cooling devices and in making solar cells, specifically, cadmium-tellurium based (CdTe) solar cells (Chivers & Laitinen, 2015). In the formulation of rubber, the metalloid is used as an accelerator and a vulcanizing agent, enhancing the formation of stronger rubber (Pale & Mamane, 2023; Rombach & Friedrich, 2014). As if this is not enough, tellurium has also found its way in ceramics and glass applications as well as in catalysis where it is used as a coloring agent and as a catalyst for producing synthetic fiber and in oil refining respectively (Pale & Mamane, 2023; Rombach & Friedrich, 2014; RSC, 2025). Furthermore, a review of the importance of tellurium by (Pale & Mamane, 2023) indicates that some compounds of the metalloid is shown to possess antitumoral, antibiotic, antiparasitic and neuroprotective effects.

However, tellurium, also listed among the critical metals in the European Union is relatively rare in its pure state and often found as a compound in ores of other elements such as copper, lead, gold, mercury, nickel, silver, zinc and bismuth (Moss et al., 2011). The recycling of the metal, although, growing steadily is still evolving (Rombach & Friedrich, 2014). This study therefore

forms part of the aims of the recycling and long-term stability of thermoelectric and magnetocaloric systems' (RecycleTEAM) project to lay the foundation for the energy and resource saving recycling of tellurium containing thermoelectric materials and systems. Traditional recycling methods for tellurium and for that matter rare metals are mostly based on the process routes used for mass metals in whose ores they are found. Operating a specific recycling method for these rare metals will not prove economical because of their low content and production volumes from the ores in which they are found. The recovery of scrap from the photovoltaic (PV) industry and to some extent end of life scrap of printed circuit boards also presents a growing stream of anthropogenic (secondary) tellurium which can be recycled through pyro or hydrometallurgical process or a combination of both.

This research, however, is focused on the recycling of the oxide of tellurium (TeO_2), which is typically a deliberately produced intermediate from the traditional recovery of tellurium through copper process route, (Chung et al., 2025) with hydrogen to obtain metallic tellurium. Hydrogen reduction of metal oxides is the application of hydrogen as a reducing agent in place of carbon with the motive of reducing carbon dioxide emission especially in the steel and iron industries. Techniques based on fluidized beds, reduction retorts and thermogravimetric analysis devices are the most common worldwide, with typical temperature range from 500 to 900 degrees Celsius (Miškovičová et al., 2024). A preliminary investigation on reduction of tellurium oxide with hydrogen by Chung *et al.,* (2025) showed conversions up to 89 % in the solid-gas phase. The study also proposed a reaction mechanism for the process based on observations made in scanning electron microscope images and recommended future studies to verify the proposed mechanism. For this study, the aim is to characterize the hydrogen reduction of tellurium oxide using experimental data and kinetic analysis to determine the mechanism of the reaction.

With this general introduction in mind, the following aspects of the thesis will be considered: (a) Chapter one, which will explore the background of the study, (b) Chapter two, which will represent the materials and methodologies employed in carrying out the objectives of the study and (c) Chapter three, in which the results from the applied methodologies will be presented and discussed.

CHAPTER 1
LITERATURE REVIEW

CHAPTER 1 LITERATURE REVIEW

INTRODUCTION

This chapter presents a review of various aspects of the topic being explored in this study. The review begins with a background of some of the specific materials used in the study, their applications, properties and production. Later, relevant literature relating to the methodology employed in this study is discussed. The chapter ends with a general review of hydrogen reduction of metal oxides both on project and laboratory scale.

1.1 TELLURIUM OXIDE

Tellurium oxide (TeO_2), scientifically known as Tellurium (IV) oxide is a solid oxide of tellurium as well as a ceramic material that can function as a semiconducting oxide, having a high mobility and a broad band gap according to calculations from density function theory (DFT) (Chemical Book, 2023). It usually exists in two distinct forms, synthetic tetragonal alpha tellurium oxide (α-TeO_2), appearing as a white solid and orthorhombic mineral tellurite (β-TeO_2), which appears as a yellow solid (AZoM, 2011; Chemical Book, 2023). The oxide occurs naturally as mineral tellurite in one of its forms (orthorhombic), which is obtained from natural deposits. Tellurium oxide can also be produced midway through tellurium metal recovery processes from electrolytic copper refining anode slimes. Another means of producing the oxide is by treating tellurium metal with nitric acid (HNO_3) and then heating the resulting product to ward off the acid or by burning tellurium metal in air. The purification process of the metal oxide involves dissolving it in sodium hydroxide, filtering and adding nitric acid until the resulting solution becomes acidic to phenolphthalein. It is then decanted and the precipitate is washed several times with distilled water and then dried at 110 ^{0}C for a day. As a white, nonflammable, dimorphic, odorless and crystalline powder, tellurium oxide is insoluble in water and has a molecular mass of 159.6 grams per mole (g/mol) (AZoM, 2011; Chemical Book, 2023; National Center for Biotechnology Information, 2025). The oxide is generally not harmful when touched but can have unhealthy repercussions when inhaled or ingested, especially in sufficient quantities. Ingested or inhaled tellurium oxide has the potential to be neurotoxic where it can lead to acute or chronic situations including peripheral neuropathy and other neurological conditions. The presence of the oxide in the body also has the potential to be reproductive toxic as well as hepatotoxic where it can lead to defects or injury to the male or female reproductive function and can cause injury and dysfunction of the

liver respectively (Gaete-Argel et al., 2021; National Center for Biotechnology Information, 2025). These potential injuries or damage can range from mild, temporary changes to severe life-threatening conditions.

Table 1.1: Summary of properties of tellurium oxide

Property	Index
Molecular formula	TeO_2
Melting point	733 ^0C
Boiling point	1245 ^0C
Molar mass	159.6 g/mol
Density	5.75 g/cm^3 (tetragonal). 6.04 g/cm^3 (orthorhombic)

Source: (AZoM, 2011; Chemical Book, 2023; National Center for Biotechnology Information, 2025).

1.1.1 APPLICATIONS OF TELLURIUM OXIDE

In the metallurgical industry, tellurium oxide can be used to produce tellurium metal while in the chemical industry, its application extends to the production of tellurium salts, telluric acid and silver telluride (Ag_2Te), a compound possessing a variety of properties that make it suitable for different applications including in thermoelectric devices. Tellurium oxide is also used in acousto-optic materials (AZoM, 2011; Chemical Book, 2023), that is devices that have the tendency to convert light into sound. These devices are very crucial and have broad applications in fields such as material processing, telecommunication, defense and scientific research. Glasses with special traits can also be produced with tellurium oxide (Chemical Book, 2023). Application of tellurium oxide also extends in fiber optics for specialized application in photonics and optical communications. Tellurium oxide is also reported to remain in the realm of affairs peculiar to specialized applications in future (AZoM, 2011), as science and technology continues to develop and make breakthroughs via research.

1.2 TELLURIUM

Tellurium, one of the elements belonging to the chalcogen group, is a rare metalloid known to be mostly found in ores of other metals, notably in deposits of sulfide, akin to volcanic processes (Pale & Mamane, 2023). The metalloid has a very low abundance where it can have a representation of about hundreds of parts per million (ppm) in the Earth (Medina-Cruz et al., 2020; Pale & Mamane, 2023). Tellurium, chemically symbolized as Te, with its nomenclature coming from the Latin word "tellus", meaning earth or ground (Ba et al., 2010), is brittle and has a grayish white appearance (Medina-Cruz et al., 2020). Generally known to occupy the 52^{nd} position on the periodic table, the metalloid, tellurium, has fifty-two (52) protons occupying its nucleus and it is in the same group with other elements such as Oxygen (O), Sulphur (S), Selenium (Se), Polonium (Po) and Livermorium (Lv). It has thirty three (33) isotopes, with mass numbers ranging from 106 to 138 (Stewart, 2017). Tellurium occurring in nature is a combination of eight (8) isotopes, with Tellurium-130 (^{130}Te) being the commonest.

1.2.1 PRODUCTION AND OCCURRENCE OF TELLURIUM

Although tellurium is sometimes discovered in its elemental or native form, it is typically found geogenically, forming ores or compounds with other metals such as gold, copper, lead, bismuth in small traces making the justification of mining solely for the metalloid impossible (Medina-Cruz et al., 2020; Moss et al., 2011). The traces of the metalloid is so small that there exist about only 5 parts per billion and 15 parts per billion of the metalloid in the crust of the Earth and in seawater respectively (Medina-Cruz et al., 2020). Trace amount of the metalloid is also contained in a variety of common sulfide minerals. Anthropogenic or secondary sources of tellurium can be derived from industrial waste from photovoltaic industries, particularly, Cadmium telluride (CdTe) photovoltaic industry as well as from end-of-life scrap of some electronic devices such as tellurium-based photoreceptors, printed circuit boards and thermoelectric materials. These secondary sources were projected to represent about 7 percent (%) of the metalloid in the year 2010 (Rombach & Friedrich, 2014).

Table 1.2: Some natural ores of tellurium

Compound/Ore	Formula	Occurrence
Calaverite	$AuTe_2$	USA, Romania, Australia

Altaite	PbTe	Central and Eastern Asia
Vulcanite	CuTe	Japan, USA, Norway, Russia
Tellurobismuthite	Bi_2Te_3	USA
Hessite	Ag_2Te	USA
Coloradoite	HgTe	Australia
Melonite	$NiTe_2$	USA

Source: (Medina-Cruz et al., 2020).

Since tellurium, like other rare metals, has low content in ores in which they are found as well as low production volumes, the traditional production processes usually follow the process routes for the rich or dominant metal in the ore like copper, iron or lead since it is economically unsuitable to operate a specific recycling process route for the metalloid (Medina-Cruz et al., 2020; Rombach & Friedrich, 2014). Following these process routes, the ores are pretreated to reduce impurities in them and then introduced into hydro or pyrometallurgical metal processing routes to increase the trace amount of the rare metal such as tellurium, in this case. By-products from such processes including anode slimes, lead/copper dross and leach residue with concentrations of about one to four percent (1 to 4 %) are then subjected to the extraction steps of the rare metal to obtain the metal content (Medina-Cruz et al., 2020; Rombach & Friedrich, 2014). Tellurium is largely amassed as a by-product of copper refining process with over ninety percent (90 %) of the metalloid produced from electrolytic copper refining anode slimes even-though not all mines of copper possess tellurium in them (Moss et al., 2011). Residues from lead refineries in addition to flue dust and gases from the smelting of ores of copper, lead and bismuth are also sources from which tellurium can be produced. Other production or isolation means of tellurium involves the employment of processes related to selenium where salts of tellurous (H_2TeO_3) and selenious (H_2SeO_3) acid solutions are obtained which are then treated with sulfuric acid to yield tellurium oxide (Brasted, 2025). The tellurium oxide can then be transformed into elemental tellurium by treating it with reducing agents such as sulfur dioxide, carbon monoxide or hydrogen (Brasted, 2025).

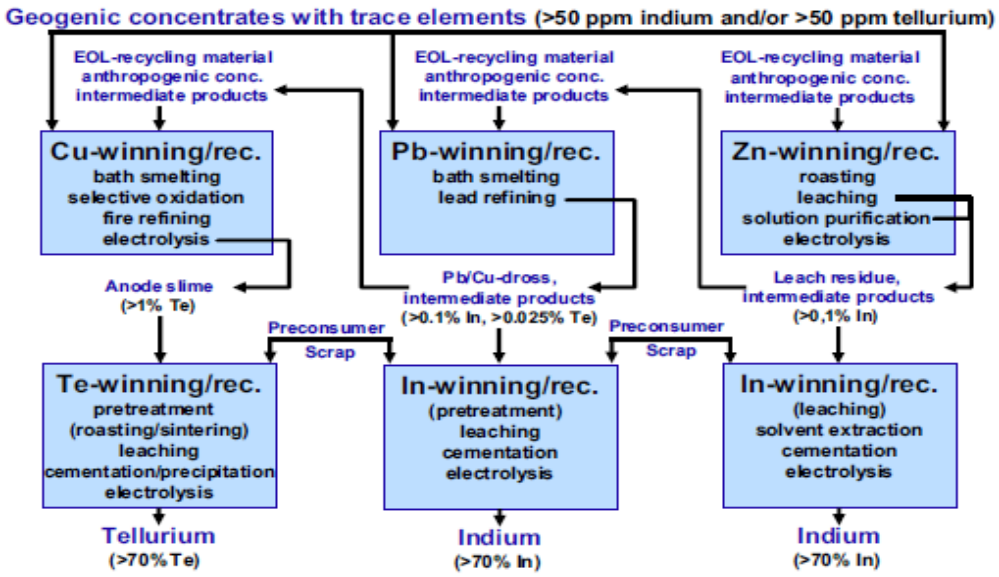

Figure 1.1: Summary of process routes for the isolation of tellurium and other rare metals
Source: (Rombach & Friedrich, 2014)

Irrespective of the unavailability of precise figures for tellurium reserves and production output, Europe is known to produce significant amounts of tellurium (Moss et al., 2011). Significant sources of telluride minerals have been discovered in the United States (US), Western Australia, China, Sweden and Mexico with China and Sweden being the two major producers of tellurium worldwide accounting for fifteen percent (15 %) of production in 2017 (Goldfarb et al., 2017; Medina-Cruz et al., 2020). Other important producers include countries like Peru and Japan (Medina-Cruz et al., 2020).

Table 1.3: Tellurium reserves in Europe based on discovered copper deposits

Country	Copper reserves (kt)	Corresponding tellurium reserves (kt)
Sweden	900	59
Portugal	1200	78
Spain	1200	78
Finland	200	13
Poland	26000	1690

Source: (Moss et al., 2011).

The market value of tellurium has experienced fluctuations over the years due to factors including but not limited to improved recovery efficiency and technologies used in the refining processes as

well as discovery of new mines. However, the price is going down with a reduction from around 225 dollars per kilogram ($225/kg) in 2010 to about 40 dollars per kilogram ($40/kg) in 2017 (Medina-Cruz et al., 2020).

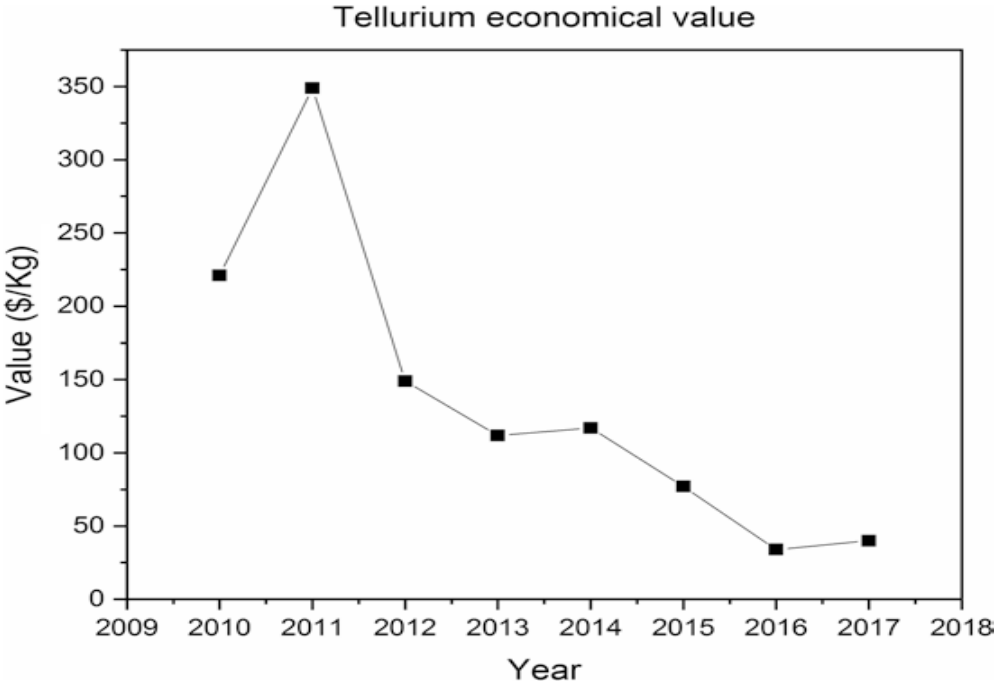

Figure 1.2: Market values of tellurium from 2010 to 2017
Source: (Medina-Cruz et al., 2020)

1.2.2 PROPERTIES OF TELLURIUM

Physically, tellurium has a silvery white appearance and its crystal structure and dimensions are similar to that of selenium. It is brittle, lustrous and conducts heat and electricity poorly and fairly respectively with its atoms forming spiral chains in its crystal with tellurium-tellurium (Te-Te) distance of 3.74 Å in its solid state. (Brasted, 2025; Stewart, 2017). However, in its liquid state, it is considered a relatively good conductor of electricity (Medina-Cruz et al., 2020). It is a semiconductor material with slight photo-sensitiveness and exceptionally rare as a result of its high volatility when it is in the hydride phase and presumed loss due to evaporation during early period when the Earth had low oxygen (Goldfarb et al., 2017; Stewart, 2017). The crystal structure of tellurium has been described to be hexagonal, orthorhombic and trigonal by different researchers (Medina-Cruz et al., 2020).

Table 1.4: Summary of properties of tellurium

Property	Index
Atomic number	52
Atomic weight	127.6
Masses of stable isotopes	120, 122, 123, 124, 125, 126, 128, 130
Melting point	449.8 ^{0}C
Boiling point	989.9 ^{0}C
Electronic configuration	$1s^2 2s^2 2p^6 3s^2 3p^6 3d^{10} 4s^2 4p^6 4d^{10} 5s^2 5p^4$
Oxidation states	-2, +2, +4, +6
Period	5
Group	16
State at 20 ^{0}C	Solid
Crystal structure	Trigonal, hexagonal or orthorhombic
Heat of fusion	17.5 kJ/mol
Heat of vaporization	48 kJ/mol
Density	6.0-6.25 g/cm^3

Source: (Brasted, 2025; Medina-Cruz et al., 2020; RSC, 2025).

1.2.3 APPLICATIONS OF TELLURIUM

The characteristics of tellurium are applied in the progress of different applications in various fields including metallurgy, energy, electronics, chemical, biological and other developing technologies. Metallurgical applications used to consume majority of the tellurium produced until recently due to the demand for solar cells. As such, applications in solar cells have increased from twenty six percent (26 %) in 2010 to about forty percent (40 %) in 2021, making applications in solar cells now the major consumer of tellurium produced (Goldfarb et al., 2017; Pale & Mamane, 2023). Another application field that has seen an increase in the consumption of produced tellurium is the application in semiconductors due to the manufacture of thermoelectric materials such as bismuth telluride used in cooling devices.

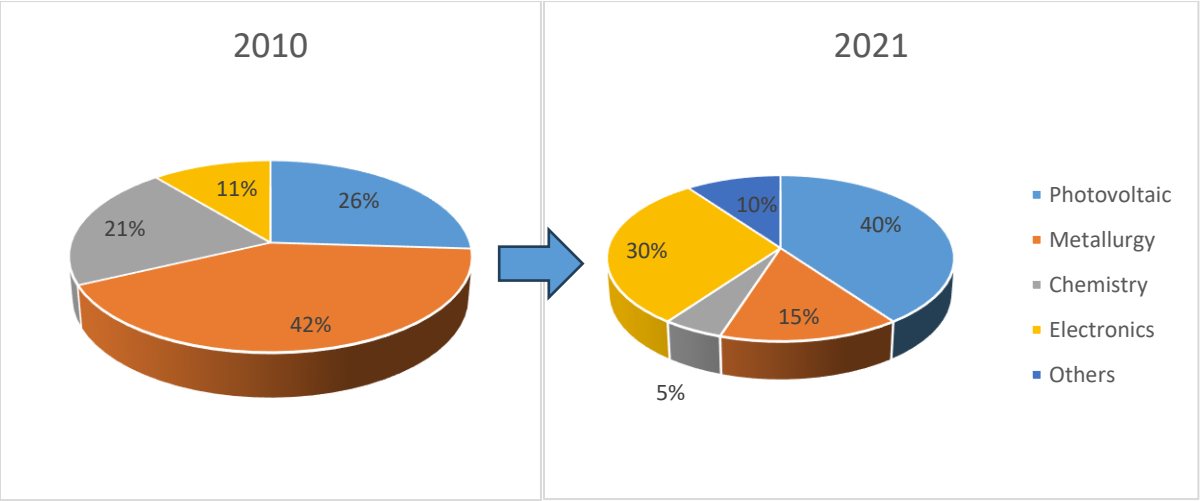

Figure 1.3: Progression in the various applications of tellurium
Data source: (Pale & Mamane, 2023)

Contrary to the above data on the consumption of tellurium by various fields, (Wei et al., 2023) reported a sixty percent (60 %) consumption for photovoltaic applications which still remains the primary consumer, a twenty percent (20 %) consumption for electronics, a ten percent (10 %) consumption for metallurgical applications and a ten percent (10 %) consumption for other applications including rubber processing and tincting of glasses and ceramics.

1.2.3.1 APPLICATION IN METALLURGY

Tellurium is applied in metallurgy as an element for alloying with the aim of improving several mechanical characteristics such as bending, shaping, and cutting of materials which are very impactful to society. It is combined with metals such as steel, copper, lead and iron to improve their performance. In copper and steel, tellurium improves the machinability of these metals (Moss et al., 2011; Rombach & Friedrich, 2014). In lead, it is used to enhance resistance to fatigue and vibration while in iron, it is used as a carbide stabilizer as well as to manage depth of chills (Medina-Cruz et al., 2020; Rombach & Friedrich, 2014).

1.2.3.2 APPLICATION IN PHOTOVOLTAICS AND ELECTRONICS

Applications here involve the use of highly purified tellurium for manufacturing semiconductor devices such as bismuth telluride (Bi_2Te_3) which can function as thermoelectric materials when combined with other elements like selenium or antimony. These thermoelectric materials can then be used for cooling applications. Another use is the manufacture of a compound which has a direct bandgap, known as Cadmium zinc telluride (CdZnTe), used in various devices such as X-ray

detectors, electro-optic modulators, solar cells and semiconductors radiation detectors (Medina-Cruz et al., 2020). Future applications here is centered on the use of tellurium to manufacture state of the art computer chips, known as phase change memory (PCM) which can store and release large amounts of energy (Medina-Cruz et al., 2020; Moss et al., 2011). In photovoltaics, where the metalloid is mostly applied, it has led to the development of cadmium telluride (CdTe) solar cells which are known to have high efficiencies compared to other solar cells, enabling power generation at comparatively low cost. These cadmium telluride solar cells on another hand have the least footprint in terms of carbon emission, water usage and energy payback period (Goldfarb et al., 2017; Medina-Cruz et al., 2020).

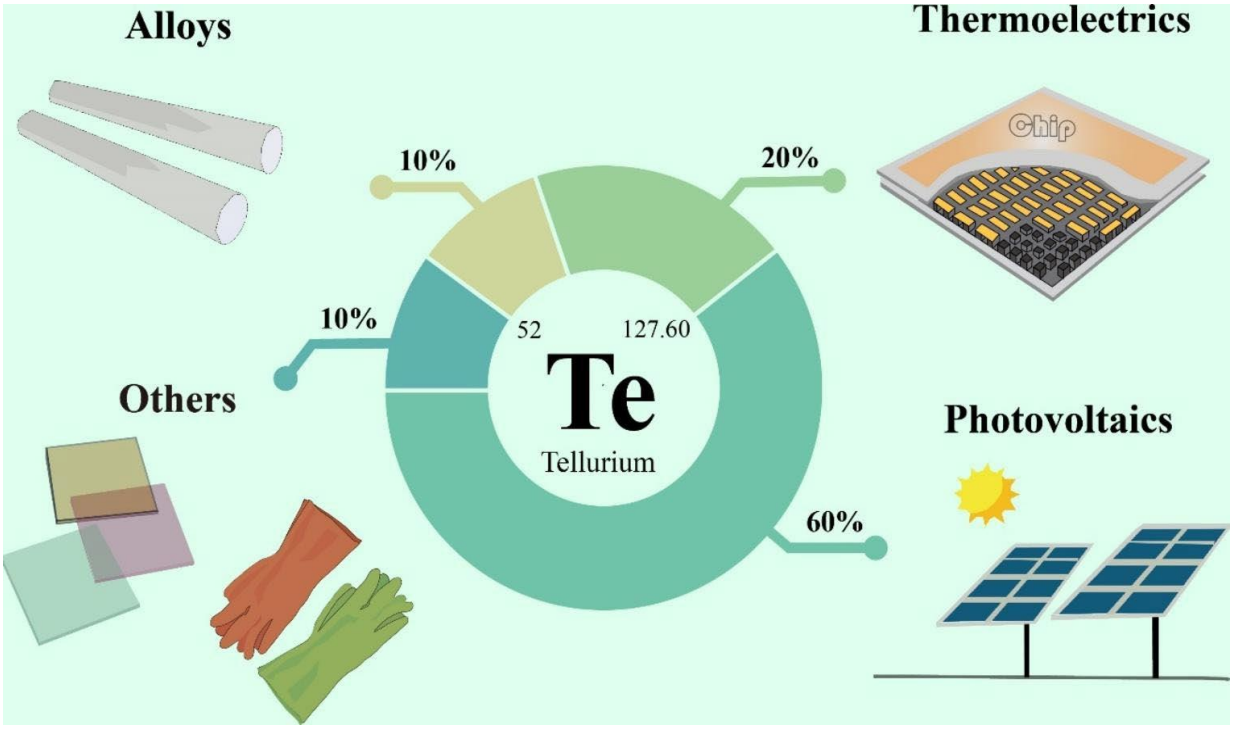

Figure 1.4: Applications for tellurium
Source: (Wei et al., 2023)

1.3 ROTARY KILN

A rotary kiln is a device broadly used in different applications due to its capability to control residence time of processed materials and to handle different loads having broad variations in their particle sizes (Bojanovský et al., 2022; Mungyeko Bisulandu & Huchet, 2023; Sun Furnace editorial team, 2025), including the manufacturing industry for producing metals such as zinc and iron, waste incineration, soil annealing and pyrolysis (Bojanovský et al., 2022). It is a conventional

technology which is well known in the cement and lime industry where it is typically applied (Bojanovský et al., 2022). The device, compared to other or general furnaces for heat treatment of materials has advantages including reduction in uneven firing during operation and likelihood of streamlining the manufacturing process (Sun Furnace editorial team, 2025). The rotary kiln, through its high temperature source of heat and exclusive mixing process can be used in various solid processes to dry, heat, incinerate, cool, calcinate, humidify, sinter and reduce materials (Bojanovský et al., 2022; Mungyeko Bisulandu & Huchet, 2023). It is versatile, as it can also be utilized to create heat treatment atmosphere suitable for raw materials by the control of temperature (Sun Furnace editorial team, 2025). The heating of a rotary kiln can be directly with the use of a burner or indirectly using electric heaters. Source of fuel for burners could be gas, liquid such as liquified petroleum gas, kerosene, heavy oil or even solid fuel (Bojanovský et al., 2022; Sun Furnace editorial team, 2025). Kilns that are electrically heated with a heater usually use gases such as hydrogen, argon, nitrogen and other gases as their processing atmospheres (Sun Furnace editorial team, 2025).

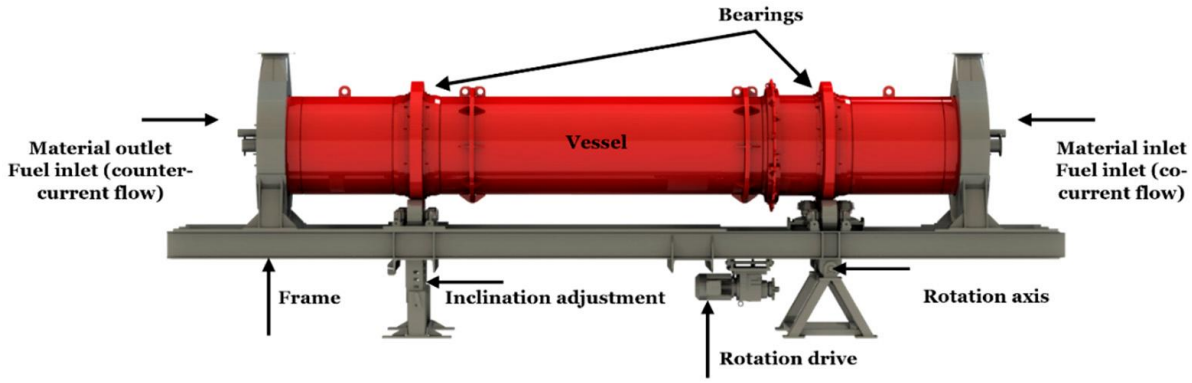

Figure 1.5: Typical layout of a rotary kiln
Source: (Bojanovský et al., 2022)

As a slightly inclined cylindrical device that rotates around its longitudinal axis, a rotary kiln sits on roller supports and also has a motion induced rotating motor (Bojanovský et al., 2022; Mungyeko Bisulandu & Huchet, 2023). The device, invented in the early nineteenth (19^{th}) century, has since undergone modifications (Mungyeko Bisulandu & Huchet, 2023) with a tilted furnace core tube (retort), inside which various materials including plastics, metals, wood chips and sludge are thermally treated while being mixed, is its main component (Sun Furnace editorial team, 2025). Various rotary kiln models, designed for unique applications and the need to enhance heat processes with different time and temperature requirement include models such as the direct flame

model which yields high efficiency for processes involving the production of cement and lime; the indirect flame model, ideal for waste treatment; the model with heat exchanger which has a system for recovering and resuing of waste heat and the model with flexible and compact design which is used in laboratories for conducting research or in pilot plants (Quiñonez, 2025).

Varied temperatures are considered during the operation of a rotary kiln and this depends on the type of material being processed. For instance, at 500 ^{0}C operating temperature, applications could include fertilizer production by drying of sludge, reprocessing of dry powdered material, drying powdered carbon; between 500 to 800 ^{0}C operating temperature, applications could include annealing of iron poweder; at around 3000 ^{0}C operating temperature, applications could be incinerating and between 800 to 1100 ^{0}C, applications could be annealing of metal powder and hydrogen reduction (Sun Furnace editorial team, 2025; Vijayan & Sendhilkumar, 2014).

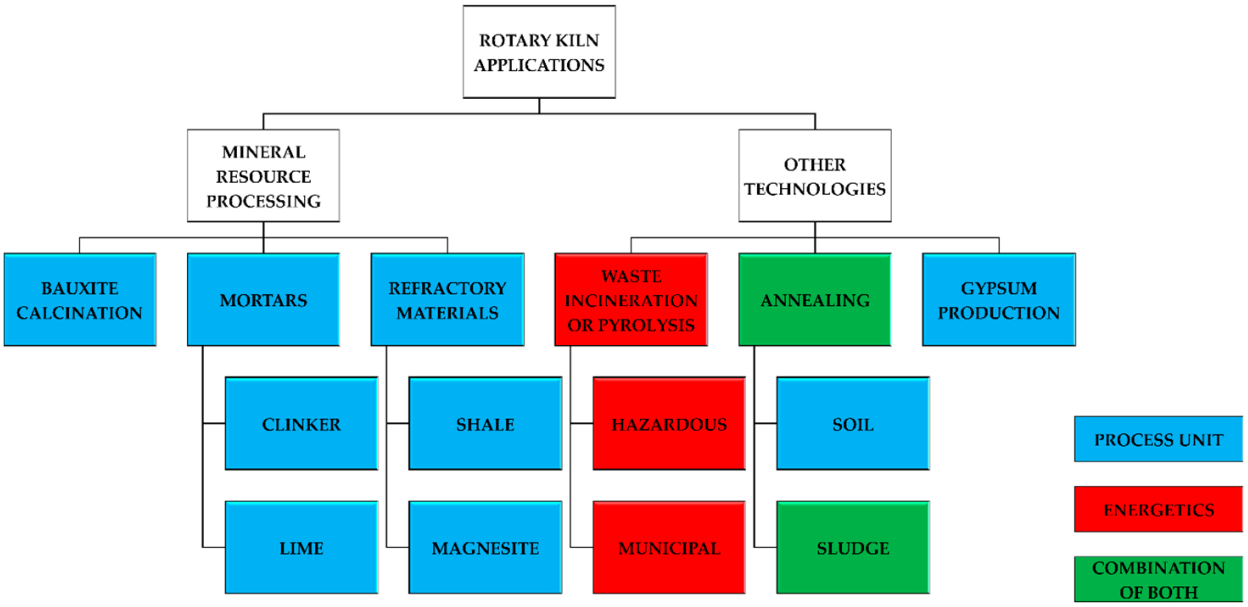

Figure 1.6: Industrial applications of rotary kiln
Source: (Bojanovský et al., 2022)

Since a rotary kiln has a motion induced mechanism which aids in the movement of the device around its longitudinal axis and consequently in the uniform mixing of materials being treated, different mixing states of the materials can be identified because of the number of revolutions involved in the movement (Friedrich, 2025; Mungyeko Bisulandu & Huchet, 2023). For small number of revolutions, usually from 0 to 0.04, there is slide convection of materials with no mixing. Moderate number of revolutions, that is between 0.04 to 0.20 corresponds to the slipping,

trickling (optimal working conditions) or rotating (good mix) of the materials. With a high number of revolutions, usually above 0.2, the mixing state of the materials is described as spinning. Finally, the materials remain on the outer wall of the kiln and have no natural movement for critical number of revolutions (Friedrich, 2025; Mungyeko Bisulandu & Huchet, 2023).

Basic form	Slipping motion		Cascading ("tumbling") motion			Cataracting motion	
Subtype	Sliding	Surging	Slumping	Rolling	Cascading	Cataracting	Centrifuging
Schematic	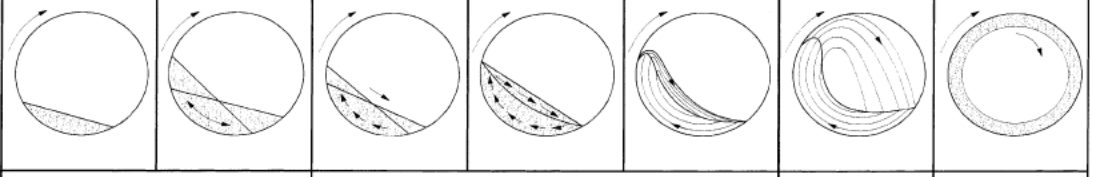						
Physical process	Slipping		Mixing			Crushing	Centrifuging
Froude number Fr [-]	$0 < Fr < 10^{-4}$		$10^{-5} < Fr < 10^{-3}$	$10^{-4} < Fr < 10^{-2}$	$10^{-3} < Fr < 10^{-1}$	$0.1 < Fr < 1$	$Fr \geq 1$
Filling degree f [-]	$f < 0.1$	$f > 0.1$	$f < 0.1$	$f > 0.1$		$f > 0.2$	
Wall friction coeff. μ_w [-]	$\mu_w < \mu_{w,c}$	$\mu_w \geq \mu_{w,c}$	$\mu_w > \mu_{w,c}$			$\mu_w > \mu_{w,c}$	
Application	no use		Rotary kilns and reactors; rotary dryers and coolers; mixing drums			Ball mills	no use

Figure 1.7: Different flow regimes or mixing states in a rotary kiln
Source: (Mungyeko Bisulandu & Huchet, 2023).

1.3.1 HEAT TRANSFER IN A ROTARY KILN

Generally, exchange of heat in a rotary kiln takes place in the three (3) known traditional modes of heat transfer (Atmaca & Yumrutaş, 2014; Mungyeko Bisulandu & Huchet, 2023). These heat transfer modes are conduction, convection and radiation. According to (Ehlmé et al., 2023), radiation heat transfer is the dominant mode at high temperatures with the total heat transfer being influenced by the processed materials and the atmosphere gases due to their absorption, emission and scattering of radiation.

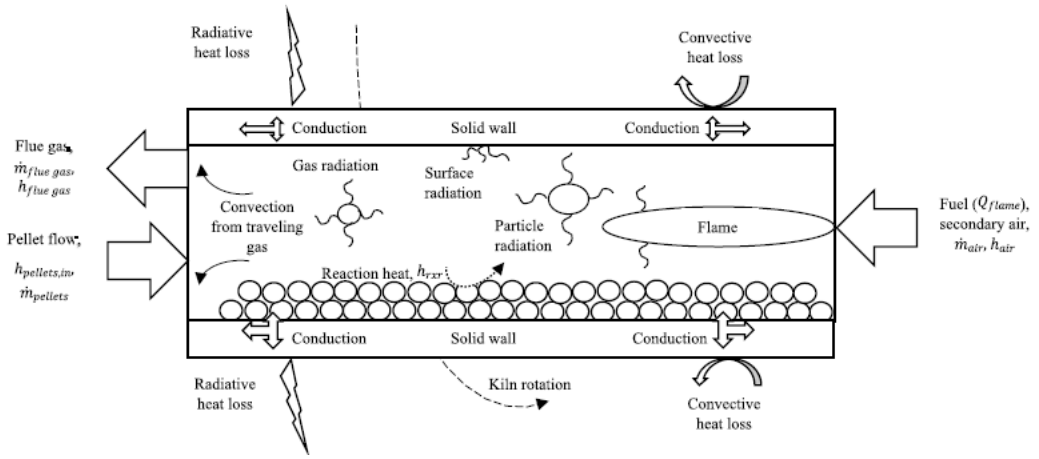

Figure 1.8: Schematic of heat transfer mechanisms in rotary kiln
Source: (Ehlmé et al., 2023)

Conduction heat transfer in a rotary kiln occurs between the kiln's covered wall and the processed materials as the materials cover portions of the wall. This mode of heat transfer could also occur within the entire wall of the kiln as the wall heats up and between the wall of the kiln and the bulk fluid (gas) which is in contact with the wall. Convection heat transfer in the kiln takes place between the atmosphere gas and the solid materials being heated, within the atmosphere gas molecules, the gas and the walls of the kiln and the outer walls of the kiln and the ambient air in contact with each other. Radiation heat transfer occurs between the atmosphere gas and the solid, the gas and the wall of the kiln, the uncovered wall of the kiln and the solid, and the outer wall of the kiln and the ambient air in contact with each other (Mungyeko Bisulandu & Huchet, 2023).

1.3.2 HYDROGEN REDUCTION IN ROTARY KILNS

Hydrogen reduction of materials, for example metal oxides in a rotary kiln is a viable approach. This can be confirmed by various studies that have explored similar procedures in the reduction of metal oxides, showing the practicality and setbacks of the process. The hydrogen reduction process is endothermic (the reaction absorbs heat from its surroundings) (Wagner et al., 2008), hence the atmosphere surrounding the reaction must have a temperature, sufficiently high enough for the reaction to take place. The rotary kiln is a device that can be employed to create this heat treatment atmosphere required for the hydrogen reduction process. This operational characteristics of the rotary kiln in addition to others such as rotating during operation, which helps the materials undergoing reduction to mix well with the reducing agent/gas (for example, hydrogen) and control of material elapsed time makes the rotary kiln suitable for hydrogen reduction processes.

Chung et al., (2025) investigated the reduction of a metal oxide (tellurium oxide) using hydrogen in an oscillating kiln furnace, with temperature ranges up to 800 ^{0}C. The results from the study showed a reduction rate of up to 89 %, signifying the practicality and feasibility of hydrogen reduction in rotary kilns. A direct reduction of iron ore using a rotary kiln was also studied by (Taheri, 1982). In the study, the author successfully converted hematite iron ore from Brazil into iron using gaseous reactants in a mixture of hydrogen, carbon dioxide and butane ($H_2/CO_2/C_4H_{10}$) as the reducing agent. Reduction percentages obtained in the study were influenced by varying operating conditions such as temperature, residence time of ore, particle size of ore, composition of reducing gases and volume of ore.

Furthermore, the characteristics of a reduction process in a pre-reduction rotary kiln was analyzed numerically by (Liu et al., 2021) where a three dimensional (3D) steady state computational fluid dynamics model, which considers mass and heat transfer as well as chemical reaction was developed. In the study, the heterogeneous reduction reaction which took place between iron oxide and a mixture of reducing gases (hydrogen and carbon monoxide) yielded a metallization rate slightly above 70 %, showing that a reduction process in a rotary kiln is viable. To conclude, a United States patent, invented by (Zeng et al., 2024), involves the use of hydrogen plasma and hydrogen gas in the direct reduction of iron ore to iron in a rotary kiln reactor. More precisely, the current invention describes a method of efficiently producing iron with absolutely no carbon dioxide emission using hydrogen gas or plasma in a rotary kiln furnace.

The highlighted reference above demonstrate that hydrogen reduction in a rotary kiln is a practical and feasible process.

1.4 KINETIC ANALYSIS

Kinetic analysis of chemical reactions refers to the investigation of the rate or extent to which a chemical reaction progresses, including factors that influence the rate. Representing an essential field of study in chemical engineering, it facilitates in the understanding of how fast a reaction takes place, what the controlling factors of the reaction are, what steps are involved in the reaction and the translation of studies performed on the laboratory scale into large or industry scale (Fedunik-Hofman et al., 2019). Kinetic analysis is relevant in the study of different processes with the acquisition of information about the mechanism of the process and determination of some kinetic parameters including activation energy and pre-exponential factor as the prime goals

(Brown, 2004). The use of reaction models for the acquisition of information about the mechanism of a process or reaction in turn ends up being useful in revising the progression or advancement of the reaction as well as envisioning the characteristics of similar reactions or processes. The determination of kinetic parameters on the other hand proves relevant in the calculation of rates of reaction for different experimental conditions other than the one from which the parameters were determined (Brown, 2004; Fedunik-Hofman et al., 2019).

Common methods employed in kinetic analysis, that is the identification of a process or reaction mechanism and determination of kinetic parameters include model-fitting of various reaction models and model free and generalized methods, which have been used to model solid-gas reactions or processes (Fedunik-Hofman et al., 2019). These common methods employed in kinetic analysis are applicable to processes including chemical ones like the thermal degradation of polymers, crystallization of glasses and thermal decomposition of solids.

1.5 SOLID-GAS REACTIONS

Solid-gas reactions are universal reactions which occur around the Earth and other heavenly bodies (King et al., 2018). These reactions are heterogeneous (require two different phases of materials) in nature and are generally described in reference to the solid and liquid phases involved in the reaction and the reaction products formed.

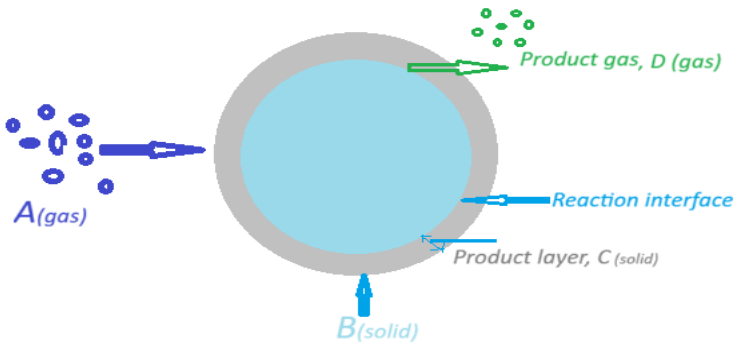

Figure 1.9: Schematic of a solid-gas reaction of the form A(gas) + B(solid) → C(solid) + D(gas)

As such, solid-gas reactions can be described or classified as a vaporization or condensation reaction, that is a solid combining with a gas to form a product gas or a solid reactant vaporizing to form gaseous products; gas release or uptake reactions, that is a solid reactant undergoing decomposition to form a solid and gaseous product (King et al., 2018). Other classifications

include gas-driven electron transfer reactions, surface mediated chemisorption reactions and catalysis reactions which in one way or the other involved either a solid and gaseous material as reactants or products (Fedunik-Hofman et al., 2019; King et al., 2018).

The means of a solid-gas reaction, whether fast, slow, linear or non-linear can be expressed by changes in conversion, that is the amount of reactant material that has been involved in the reaction, with time and since a solid-gas reaction proceeds with the absorption or release of a gas, the conversion can be determined by changes in mass before and after the reactions (Fedunik-Hofman et al., 2019). The conversion is regularly professed on fraction bases and its expression depends on whether the solid-gas reaction involves a mass loss or mass gain. For a reaction involving a mass loss, the conversion can be expressed as:

$$\alpha = \frac{m_i - m_f}{m_i \, E_m} \tag{1}$$

where α is conversion, m_i is initial mass, m_f is final mass, E_m is mass fraction of solid effectively involved in the reaction and $m_i > m_f$. For a reaction involving a mass gain, the conversion can be expressed as:

$$\alpha = \frac{m_f - m_i}{m_f \, E_m} \tag{2}$$

where α is conversion, m_i is initial mass, m_f is final mass, E_m is mass fraction of solid effectively involved in the reaction and $m_f > m_i$. The conversion values change with time as the reaction proceeds and can have a characteristic curve. Kinetic models for solid-gas reactions are normally used to comprehend these curves and also relate them to various mechanisms involved in the reaction (Fedunik-Hofman et al., 2019).

The reactions involving solids and gases are broadly employed in various processes or fields including metallurgy, chemical, energy and materials and are typically influenced by factors, with emphasis on the solid, such as the transportation of gas to solid, adsorption of the gas on the surface of the solid and the evolution of the process that occurs between the gas and solid (King et al., 2018; Z. Li, 2020).

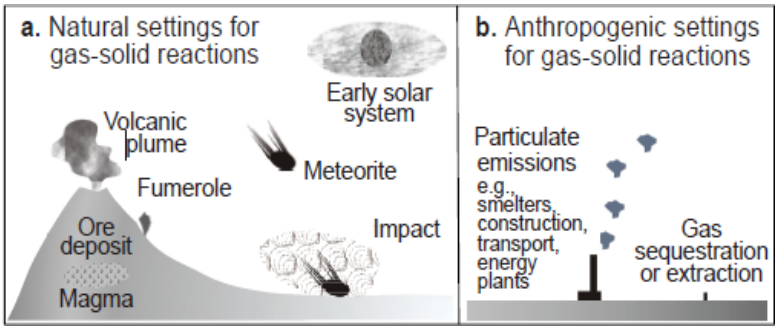

Figure 1.10: Natural and artificial settings for solid-gas reactions
Source: (King et al., 2018).

1.5.1 SOLID-GAS REACTION MODELS

A plethora of reaction models, which are a mathematical translation of the progress mechanism of a reaction have been developed and tried out. The development of these models is based on the theory of a reaction mechanism or by empirical fitting with minimal physical meaning (Dhyani & Bhaskar, 2018). Papamichael et al., 2019 also reported that reaction models can be constructed based on reasonable hypotheses as well as on collecting series of data, organizing and illustrating them. The Models can be classified as acceleratory, deceleratory, linear or sigmoidal. This classification is based on the shape of a reaction isotherm. A reaction isotherm could be a plot of conversion against time or change in conversion with time against time. Models such as diffusion models, geometrical contraction models, nucleation or growth models and order-based models are also classified based on assumptions of the mechanisms of various reactions (Dhyani & Bhaskar, 2018; Khawam & Flanagan, 2006)

Table 1.5: Some known reaction models

Reaction Models	Classification
Avrami-Erofeev	Nucleation and Growth
Shrinking Core (Diffusion)	Diffusion
Shrinking Core (Reaction)	Surface reaction
Ginstling-Brounshtein	Diffusion
First Order	Order-based
Second Order	Order-based
Jander	Diffusion
Contracting Volume	Geometric Contraction

Prout-Tompkins Model	Autocatalytic Reaction

Source: Adapted and modified from (Dhyani & Bhaskar, 2018).

1.5.1.1 AVRAMI-EROFEEV REACTION MODEL

The Avrami-Erofeev model is used to model the progress in a material's phase transformation such as crystallization and thermal decomposition. It was deduced independently in the mid twentieth century by Robert Mehl and his student W. Johnson, Melvin Avrami and Andrei Kolmogorov (Cantor, 2020; Shirzad & Viney, 2023). As such, the model is sometimes referred to as JMAK equation. The equation, which is a simple sigmoidal function expresses transformation fraction as a function of time. The equation is expressed as:

$$\propto = 1 - e^{(-kt^n)} \tag{3}$$

where $\propto$ represents fraction of material transformed (which is a function of time), t represents time whereas k and n represent constants which are extracted from the model (Shirzad & Viney, 2023). The equation (1) above can further be transformed into a linear form to obtain:

$$(-\ln(1-\propto))^{\frac{1}{n}} = kt \tag{4}$$

Comparing equation 2 to the general form of an equation of a line ($y = mx +$ c) and with the values of $\propto$ and t obtained from experiments, the constants k and n can be obtained from a plot of $\propto$ versus t. The constant k is a function of nucleation and growth rate involved in the phase transformation of a material system. The constant n depends on the instantaneity and sporadicity of nucleation as well as the dimensionality of growth. The nucleation component of the constant n is 0 or 1 for instantaneous or sporadic nucleation respectively while the growth component is 1, 2 0r 3 (growth due to interfacial migration) or 3/2, 1 or ½ (growth due to diffusion) for one dimensional, two dimensional or three dimensional growth respectively (Shirzad & Viney, 2023).

The development and application of the Avrami model has not been restricted to only material system but also in other research fields such as life sciences. This is possible because some systems from these research fields can be considered as undergoing a phase transformation and there is the possibility of identifying non-thermodynamic impetus similar to supersaturation and undercooling in the systems of these fields (Shirzad & Viney, 2023). Included in other research fields where the Avrami model has been applied are cancer studies, genetics studies, biochemical processes, ecology, epidemiology, chemistry, social studies and product market analysis.

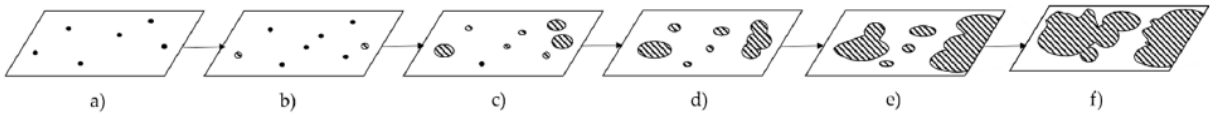

Figure 1.11: Avrami-Erofeev model (Nucleation and growth model): (a) nucleation sites, (b) first nuclei formed, (c) growth and further nucleation, (d) overlap of nuclei, (e) ingestion of nucleation site, (f) continued growth
Source: (Fedunik-Hofman et al., 2019).

1.5.1.2 SHRINKING CORE REACTION MODEL

The Shrinking Core Model is the most widely utilized model among the models developed for non-catalytic reactions between fluids and solids. The development of the model took into account some considerations including the solid reactant being a non-porous material initially engulfed by a film of fluid, the gaseous or liquid reactant, through which interaction occurs (mass transfer) between the large volume of the fluid and the solid material (Gbor & Jia, 2004). The reaction between the solid particle and fluid reagent leaves behind a reacted, inert or consumed layer around an unreacted core. The equation below, adapted from (Sloman et al., 2019) is the universal or common chemical reaction (irreversible) used in the establishment of the Shrinking Core Model.

$$A_{gas} + \sigma_1 B_{solid} \rightarrow \sigma_2 C_{gas} + \sigma_3 D_{solid} \quad (5)$$

From the reaction, σ_1, σ_2 and σ_3 are stoichiometric coefficients. The model also postulates that the reaction occurs at an interface between the reacted layer and unreacted core of the solid particle and moves towards the center of the unreacted core until the reaction is complete (Melchiori & Canu, 2014; Sloman et al., 2019). As the reaction is a multi-step one, different controlling regimes, that is steps that control how fast the overall reaction can proceed determine the form of the rate equation of the Shrinking Core Model. The different controlling regimes or steps as described by (Gbor & Jia, 2004), (Sloman et al., 2019) and (Melchiori & Canu, 2014) are diffusion through the reacted or inert solid layer and chemical reaction at the interface between the reacted layer and unreacted core of the solid particle. These controlling regimes therefore give rise to what is described as Diffusion Shrinking Core Model and Reaction Shrinking Core Model.

1.5.1.2.1 DIFFUSION SHRINKING CORE MODEL

This is a model used to describe reactions between fluids and solids where diffusion through the solid particle is the slowest step. Since the reaction occurs in multiple steps, this implies that the overall reaction between the fluid (eg. gas) and the solid particle depends on how quickly the fluid

diffuses through the inert, reacted or product layer of the solid to encounter the unreacted core of the solid for the reaction to progress. This also hints that the chemical reaction here is faster than the diffusion process. The equation for this Shrinking Core Model, obtained from (Gbor & Jia, 2004; Sloman et al., 2019) is given as:

$$kt = 1 - 3(1 - x)^{\frac{2}{3}} + 2(1 - x) \quad (6)$$

where k is rate constant, t represents time and x is conversion or fraction of solid transformed. Gbor & Jia, 2004 reported that this equation might be unapplicable to solid-liquid reactions because it was derived from an approximation which is valid if the ratio of the concentration of the reactant fluid to the density on molar basis of the solid reactant is less than a fraction of $\frac{1}{1000}$ which generally applies to solid-gas reactions and not always to solid-liquid reactions. However, later studies showed that the approximation is still valid for ratios greater than the above for solid-liquid reactions by considering a convective factor to mass transfer.

1.5.1.2.2 REACTION SHRINKING CORE MODEL

Just as the name suggests, this model is used to describe or determine reactions between fluids and solids where the surface chemical reaction is the controlling regime. The implication here is that the surface chemical reaction is the step that defines how the overall chemical reaction between the fluid and solid particle will proceed and as such, the reaction process is much slower than the diffusion process. The mathematical translation for this chemical reaction, retrieved from (Gbor & Jia, 2004; Melchiori & Canu, 2014; Sloman et al., 2019) is stated below.

$$kt = 1 - (1 - x)^{\frac{1}{3}} \quad (7)$$

where k is reaction rate constant, t represents time and x is conversion or fraction of solid transformed.

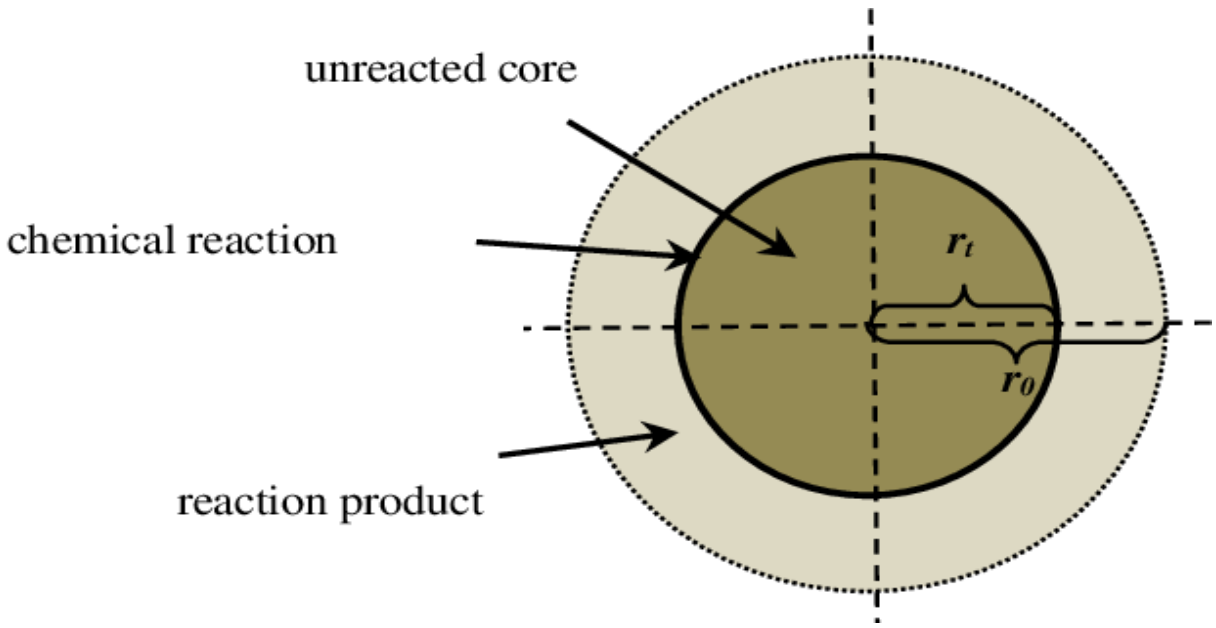

Figure 1.12: Schematic of the Shrinking Core Model
Source: (Paunović et al., 2019)

Shrinking Core Model is applied to various fluid-solid reactions that occur in different chemical processes. Included in the chemical processes where these reactions are encountered are the burning of solid fuel particles, control of gaseous pollutants, production of catalyst and in the field of metallurgical engineering (Gbor & Jia, 2004). Typical examples of these chemical processes include oxidation of metals and reduction of metal oxides using reducing gases such as carbon-monoxide or hydrogen to yield metal oxides and metals respectively. There is also the production of synthetic gas from the reaction between carbon and water vapor and the extraction of metals from ores through leaching by using acidic mediums such as studies form (Paunović et al., 2019) and (Behera & Sukla, 2012).

1.5.1.3 JANDER REACTION MODEL

The Jander model is used to describe the degree of reaction for a reaction that has a well-established principle as that of a shrinking core reaction. The model mathematically translates the extent to which the surface of a solid particle shrinks after a chemical reaction in which diffusion of reactants through an inert layer is the rate limiting step (Jander, 1927; Provis, 2016). In the said chemical reaction, the reaction takes place instantaneously at an interface unlike the diffusion process and the inert or product layer replaces the gap occupied by the initial reactant solid particle

(Provis, 2016). To mathematically translate the reaction, assumptions including but not limited to the following were considered:

i. The reaction takes place due to the possibility of diffusion of reactants.
ii. The extent of reaction is inversely proportional to time as defects in the solid increase.
iii. The rate of buildup of a new product layer is inversely proportional to the already existing product later.
iv. Only one component can diffuse through the product layer.

Other assumptions in addition to the above, described in (Jander, 1927; Khawam & Flanagan, 2006; Provis, 2016) are depicted in the figure 1.13 below.

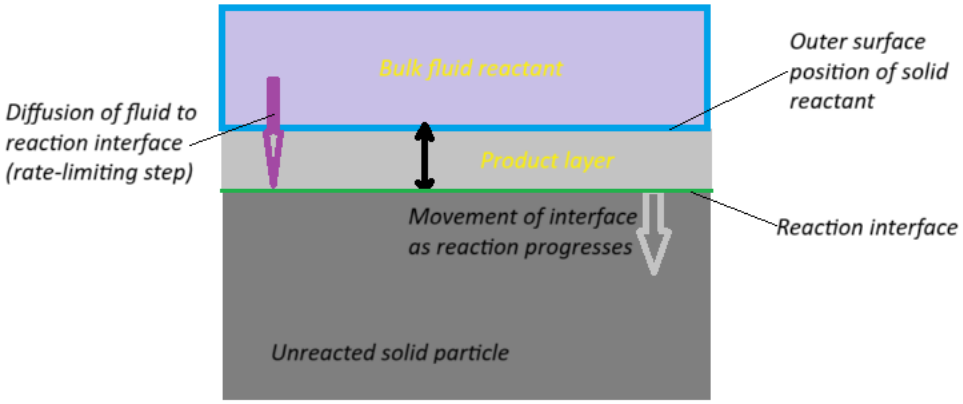

Figure 1.13: Illustration of the assumptions for deriving the Jander equation
Adapted from (Provis, 2016)

The derived equation obtained from (Khawam & Flanagan, 2006; Provis, 2016) is given as:

$$\frac{kt}{R^2} = \left(1 - (1-\propto)^{\frac{1}{3}}\right)^2 \quad (8)$$

where t represents time, k is a constant, R is initial radius of a solid reactant particle and α represents conversion.

The model is applied in cement chemistry for describing the consumption rate of a solid grain particle during a hydration chemical reaction process (Provis, 2016). The model has been criticized by different researchers due to some approximations made in the derivation of the model equation. In the derivation of the model equation, a substitution for conversion, defined in spherical coordinated was made into an equation for conversion derived from cartesian plane or coordinated. Previous studies including (Provis, 2016) describe this approximation as a neglect of surface

curvature of particle and hence the use of the model for any interaction over a minute extent of reaction is incorrect.

1.5.1.4 GINSTLING-BROUNSHTEIN MODEL

The Ginstling-Brounshtein model, just as the Jander model describes the rate of reaction of a chemical process which is limited by diffusion. The model is based on the theory that the volume of the product layer is the same as that of the unreacted layer, signifying that the ratio of the volume of the reactant to that of the product is unity (Satoshi, 2019). The model is also based on similar assertions as that of the Jander model including but not limited to the surface reaction occurring very quickly in comparison with the diffusion process as well as the reacted or inert layer uniformly covering the unreacted particle surface.

However, in the derivation of the equation, the substitution of conversion defined in spherical coordinated was made into a similar equation also defined in the same coordinate, thereby taking into account the surface curvature of the particle involved, unlike the Jander model (Provis, 2016). This then makes the Ginstling-Brounshtein model a preferred model for use if the inference of diffusion control and other factors such as particle size remaining the same leads to the choice of the Jander model (Provis, 2016).

The derived equation for the model, sourced from (Krauklis & Dreyer, 2018; Satoshi, 2019) is given as:

$$\frac{kt}{R^2} = 1 - \frac{2\alpha}{3} - (1-\propto)^{\frac{2}{3}} \tag{9}$$

where k represents the kinetic constant, t represents time, R represents the particle radius and α represents conversion.

As reported by Krauklis & Dreyer (2018), the practical application of the Ginstling-Brounshtein model has been studied and documented for different applications including hydration and dehydration processes, solid state synthesis processes, thermal degradation processes, just to mention a few.

Table 1.6: Summary of some reaction models

Model	Integral form	Plot of linearity	Rate-limiting step

Avrami-Erofeev	$kt = (-\ln(1-\propto))^{\frac{1}{n}}$	lnt versus $\ln(-\ln(1-\propto))$	Nucleation and growth
Diffusion Shrinking Core	$kt = 1 - 3(1-\propto)^{\frac{2}{3}} + 2(1-\propto)$	t versus $1 - 3(1-\propto)^{\frac{2}{3}} + 2(1-\propto)$	Ash-layer diffusion
Reaction Shrinking Core	$kt = 1 - (1-\propto)^{\frac{1}{3}}$	t versus $1 - (1-\propto)^{\frac{1}{3}}$	Surface reaction
Jander	$kt = \left(1 - (1-\propto)^{\frac{1}{3}}\right)^2$	t versus $\left(1 - (1-\propto)^{\frac{1}{3}}\right)^2$	Product layer diffusion
Ginstling-Brounshtein	$kt = 1 - \frac{2\alpha}{3} - (1-\propto)^{\frac{2}{3}}$	t versus $1 - \frac{2\alpha}{3} - (1-\propto)^{\frac{2}{3}}$	Product layer diffusion

1.5.2 MODEL FREE KINETIC ANALYSIS METHODS

Model free kinetic analysis methods require multiple data sets and help in the calculation of activation energy (E_a) with no dependency on a reaction model. These methods also help in the identification of multi-step processes involved in a reaction. The kinetic parameters obtained using these methods are usually determined over a range of conversion between 0.05 and 0.95 (Fedunik-Hofman et al., 2019). These methods include the iso-conversional methods and the Kissinger method.

1.5.2.1 ISOCONVERSIONAL METHODS

The iso-conversional methods are based on the iso-conversional principle. The principle states that at constant conversion extent, the rate of reaction is a function of temperature only. This implies that without assuming any reaction model, the dependence of the reaction rate on temperature can be used to determine the constant conversional value of the activation energy. When the activation energy significantly varies with the conversion, it implies that the process is kinetically complex and a single step rate equation cannot be applied to describe the process. The temperature dependence of the iso-conversional rate can be experimentally obtained from performing series of runs between three to five at various temperature regimes or heating rates or even at different constant temperatures (Vyazovkin et al., 2011). Iso-conversional methods are broadly split into two types namely differential and integral iso-conversional methods.

1.5.2.1.1 DIFFERENTIAL ISOCONVERSIONAL METHODS

The Friedman method is the most common differential iso-conversional method (Vyazovkin et al., 2011). It is based on applying the iso-conversional principle to the general rate equation. The derived equation after applying the principle, obtained from Vyazovkin *et al.,* (2011) is shown below.

$$\mathbf{ln}\left(\frac{d\propto}{dt}\right)_{\propto,i} = \mathbf{ln}[f(\propto)A_{\propto}] - \frac{E_a}{RT_{\propto,i}} \tag{10}$$

E_a is activation energy, R is gas constant, $T_{\propto,i}$ is temperature at which the extent of conversion (α) is reached under the $,ith$ temperature program and the index i denotes the different temperature programs (that is the individual temperature for isothermal temperature programs and individual heating rate for non-isothermal program).

The value of the activation energy E_a is determined from the plot of $\ln\left(\frac{d\propto}{dt}\right)_{\propto,i}$ versus $\frac{1}{T_{\propto,i}}$ at every given α. For a non-isothermal program, $T_{\propto,i}$ is assumed to linearly differ with time with reference to the heating rate (βi) and the equation is therefore used in the form shown below.

$$\mathbf{Ln}\ [\beta i(\frac{d\propto}{dT})_{\propto,i}] = \mathbf{ln}[f(\propto)A_{\propto}] - \frac{E_a}{RT_{\propto,i}} \tag{11}$$

The differential iso-conversional methods are considered more accurate than the integral methods because the former avoid the use of approximations. However, certain imprecisions and inaccuracies are inevitably associated with the practical use of the differential method. For instance, when the method is applied to differential data such as DTA and when the reaction heat reveals a clear dependence on the heating rate. Also when the method is applied to integral data, the use of numerical differentiation creates imprecisions in the rate data which may result in inaccuracy during smoothing of the data (Vyazovkin et al., 2011).

1.5.2.1.2 INTEGRAL ISOCONVERSIONAL METHODS

The Integral iso-conversional methods are based on applying the iso-conversional principle to the integral form of the general rate equation. The equation is rearranged after simplification to obtain the equation shown below, obtained from (Vyazovkin et al., 2011).

$$\ln t_{\propto,i} = \ln\left[\frac{g_{(\alpha)}}{A_{\propto}}\right] + \frac{E_{\alpha}}{RT_i} \tag{12}$$

The parameter, $t_{\propto,i}$, represents the time to reach a given conversion extent at different temperature, T_i for isothermal temperature condition. From the slope of a plot of $\ln t_{\propto,i}$ against $\frac{1}{T_{\propto,i}}$, the value of the activation energy E_a can be determined. For constant heating rate condition, the time is replaced by temperature and the corresponding heating rate and the equation is approximated to form a linear equation shown below, sourced from (Fedunik-Hofman et al., 2019; Vyazovkin et al., 2011).

$$\ln\left[\frac{\beta i}{T^{B}_{\propto,i}}\right] = Const - C\left(\frac{E_{\alpha}}{RT_{\alpha}}\right) \tag{13}$$

The constants B and C are parameters determined from the category of the temperature integral approximation. B and C are approximated to 0 and 1.052 respectively, making the equation take a form shown below, known as the Flynn and Wall and or Ozawa equation.

$$\ln(\beta i) = Const - 1.052\left(\frac{E_{\alpha}}{RT_{\alpha}}\right) \tag{14}$$

1.5.2.2 THE KISSINGER METHOD

Among the multi-heating methods for determining activation energy, the Kissinger method is the most applied method because it is simple to use (Fedunik-Hofman et al., 2019; Vyazovkin et al., 2011). The method is based on the general rate equation under the condition of maximum rate of reaction. At maximum rate of reaction, the second derivative of the rate equation is equated to zero. This yields the equation shown below, obtained from (Vyazovkin et al., 2011).

$$\frac{E\beta}{RT_m^2} = -Af'^{(\alpha_m)}\exp\left(\frac{-E}{RT_m}\right) \tag{15}$$

The term $f'^{(\alpha_m)} = \frac{df(\propto)}{d\propto}$ while the subscript m represents the maximum rate values. The equation is further rearranged to form the Kissinger equation shown below.

$$\ln\left[\frac{\beta}{T^2_{m,i}}\right] = \ln\left[-\frac{AR}{E}f'^{(\alpha_m)}\right] - \left(\frac{E}{RT_{m,i}}\right) \tag{16}$$

From the Kissinger equation above, a plot of $\ln\left[\frac{\beta}{T^2_{m,i}}\right]$ against $\frac{1}{T_m}$ yields a straight line. The activation energy is then determined from the slope of the straight line. The Kissinger method, even though it is simple to use has some limitations. One of them is that the term $f'^{(\alpha_m)}$ in the

equation must be independent of the heating rate, making the first term on the right side of the equation constant. This helps to produce accurate value of activation energy. Another limitation of the Kissinger method is that irrespective of how complex a process is, the method produces a single activation energy value for the process. It is therefore imperative to use iso-conversional method to verify the results from Kissinger method (Vyazovkin et al., 2011).

1.6 HYDROGEN REDUCTION IN METALLURGY

Hydrogen reduction in metallurgy refers to the application of hydrogen either in its gaseous or plasma state as a reducing agent for metallurgical processes such as extraction of metals from their ores or converting metal oxides into their metallic form and the production of steel (Miškovičová et al., 2024; Tang et al., 2020). The process is attracting significant attention because it represents a promising technology for sustainable and cleaner metal production, replacing conventional methods which usually involve the use of carbon and consequently production of carbon dioxide which is harmful to the environment in excess amount.

Several advances have been made regarding the use of hydrogen reduction in metallurgy both in research and projects across the world. The advances include the design and implementation of projects that use hydrogen as a reducing agent to replace conventional ones such as carbon monoxide in the production of steel and other metals. Various studies have also explored the feasibility of applying hydrogen reduction in metallurgy for the production or recycling of metals from their ores or various waste streams. The focus of these advancements is motivated by the need to pave the way for the introduction and use of suitable reducing agents and energy sources which are environmentally friendly in the metallurgical sector (Miškovičová et al., 2024).

Considering advances made in the application of hydrogen reduction in projects across the world, the Hydrogen Breakthrough Ironmaking Technology (HYBRIT) project in Sweden is one example. The project involves the development of a hydrogen direct reduced iron production technology. Completed preliminary investigations on the project show that the proposed technology is both technically and economically viable (Miškovičová et al., 2024; Pei et al., 2020). The technological setup for the project is designed to utilize hydrogen as the main reducing agent with the possibility of using other gases including biogas. The first demonstration plant for the

project was initiated in 2019 with the project being scheduled to begin operation in this year (Pei et al., 2020).

Another example is the Carbon dioxide Ultimate Reduction System by innovative technology for cool Earth 50 (COURSE50) national project in Japan. The project involves two main technologies including a hydrogen-rich reduction of iron ore and carbon dioxide capture and recovery from the exhaust of a blast furnace (Nomura, 2021). The hydrogen-rich reduction is based on the reforming technology of coke oven gas which leaves a carbonization chamber at a high temperature (800 ºC), making the cracking of tar and other hydrocarbon substances possible and consequently producing hydrogen gas. The carbon dioxide capture is based on the utilization of waste heat through an efficient carbon dioxide absorption technology (Tang et al., 2020). With the industrial trial of the technology completed, this modification will increase the hydrogen content of the coke oven gas up to 67 % with a total carbon dioxide reduction target of 30 % (Nomura, 2021; Tang et al., 2020).

Exploring further, the HELIOS project also presents a significant advancement as it seeks to produce essential human resources needed to achieve the climate-neutral production of steel by 2050 in some parts of Europe. The project, with a timeline of 2023-2027, seeks to train ten (10) doctoral candidates in state of the art technologies for the production of green steel using hydrogen (European Commission, 2023; Miškovičová et al., 2024). This aim of the project is sought to be achieved through advanced doctoral research projects, mentorship and internships. This will be done in collaboration with companies and universities including Tata Steel, SSAB Europe Oy, KU Leuven, TU Delft and research centers such as K1-MET (European Commission, 2023). This intersectoral training provided to the candidates is mainly dedicated to overcoming both technical and economic challenges as well as provide innovative developments geared towards transitioning to hydrogen based steel production (European Commission, 2023).

Other projects like Hydrogen as Reducing Agent in the Recovery of metals and minerals from metallurgical waste (HARARE) and Salzgitter Low Carbon dioxide Steelmaking (SALCOS) also represent important advancement. Both projects advocate the use of hydrogen as a substitute for carbon to make the metallurgical industry and processes greener. The HARARE project is aimed at recovering waste from metallurgical processes (aluminium and copper production) with hydrogen and achieving an environmentally friendly metal industry through application of hydrogen-based processes (European Commission, 2021). The SALCOS project aims to produce

green hydrogen from water electrolysis using wind energy. The green hydrogen will then be used as a reducing agent in steelmaking processes (Zhang et al., 2021).

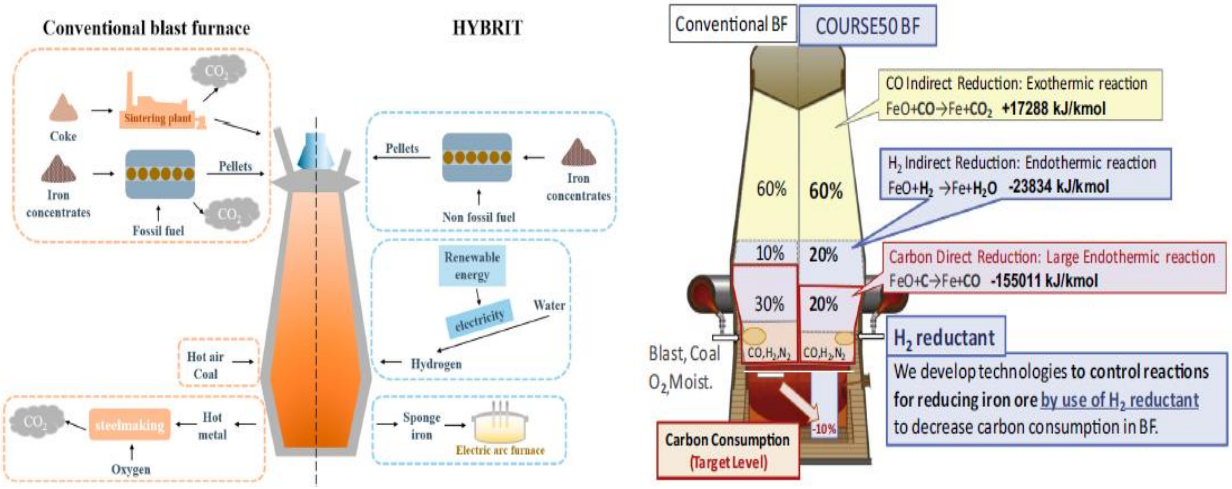

Figure 1.14: Concept of HYBRIT (left) and COURSE50 (right) projects
Source: (Nomura, 2021; Zhang et al., 2021).

Considering advances made in the application of hydrogen reduction in research, Wagner et al., (2008) investigated the reduction of iron oxide (hematite) to iron by hydrogen at laboratory scale in a thermobalance. Their investigation involved varying conditions of the experiments performed as well as observing both the rate and progress of the reaction by interrupting the experiments before complete conversion is reached. They found out that the reduction process followed a sequential order from hematite to magnetite to wustite and finally to iron, depicting a clear evolution of the samples. Luidold & Antrekowitsch, (2007) demonstrated through an overview that it is thermodynamically possible to produce metals through hydrogen reduction of their oxides, chlorides, sulfides and fluorides. They concluded their overview by highlighting that except for metals found from the second to the fifth group, most metals can be produced from their corresponding oxides by reduction with hydrogen. At the reduction temperature, the metals can be obtained as solids in powdery form, liquids such as Gallium, Indium or gases including Potassium, Sodium and Zinc.

The kinetics involved in the hydrogen reduction of lead oxides to lead was studied by Ivanov et al., (2015) within the temperature range of 450 to 525 ºC in a set-up consisting of a reaction chamber, chromatograph, signal recording system, heater, piston and a sample boat. The authors found out that the activation energy of the reduction of tetragonal lead oxide is equal to that of

orthorhombic lead oxide which are 93 ± 5 and 85 ± 8 kJ/mol respectively within the measurement error. The authors also revealed that the reactivity of both oxides with hydrogen is practically equal within the temperature range studied. It was concluded from the study that, the orthorhombic lead oxide's degree of reduction dependence on reaction time followed the Erofeev equation.

The hydrogen reduction of tungsten blue oxide to tungsten powder was investigated by Haubner et al., (1983) at temperatures of 750 and 1000 ºC with the aim of finding the mechanism of the reduction of tungsten. The investigation involved interrupting, isolating and characterizing intermediates which occurred during the reduction process. The investigation revealed that the transition involved in the hydrogen reduction of tungsten oxide to tungsten powder was from $WO_{2.9x}$ to $WO_{2.9}$ to $WO_{2.72}$ to WO_2 and finally to W. The study highlighted that the transition steps were characterized by both color and crystal morphology changes revealed by SEM. Schulmeyer & Ortner, (2002) found out from their study on the mechanism of hydrogen reduction of molybdenum oxides in a thermal balance that the process involved two stages. The first stage which obeyed the crackling core model revealed a reaction path of MoO_3 to Mo_4O_{11} to MoO_2. The Mo_4O_{11} and MoO_2 formed showed different size distribution and shape because of the local partial pressure of water during the reaction. The second stage of the reduction process which developed according to the shrinking core model was from MoO_2 to Mo with no intermediate occurring between them.

Further exploration on the hydrogen reduction of oxides led to the investigation on the kinetics of hydrogen reduction of nickel oxide at moderate temperature by (Lee & Min, 2019). In the investigation, thermogravimetric analysis experiment was used to confirm the dependence of both temperature and particle size on the reduction behavior of the oxide from micro scale to nano scale. The investigation also confirmed that the reduction of nickel oxide follows the second Avrami model with the rate of reduction capable of being expressed by function of temperature and the powder's particle size. Tomić-Tucaković et al., (2012) performed a thermogravimetric study of the kinetics of hydrogen reduction of cobalt oxide to metallic cobalt at different constant heating rates and confirmed a two-step reduction process. The two-step transformation was revealed by the differential TG curves as Co_3O_4 to CoO and from CoO to Co, confirming other literature reports. The results from the study also revealed that the granulation of oxides and final reduction

temperature influenced the mean dimension of the resulting metal particles. The study concluded that the Prout-Tompkins equation fitted best the data from the thermogravimetric experiment.

By using synchrotron based x-ray diffraction, Kim et al., (2004) investigated the reaction of copper oxides with hydrogen to ascertain the reduction mechanism and the ionic states of copper. The authors found out that under an experimental condition of normal hydrogen flow, copper oxide (CuO) directly reduces to metallic copper (Cu). Conversely, under an experimental condition of very small hydrogen flow and fast heating rate, above 20 ºC per minute, the reduction processed involved a suboxide, copper (I) oxide (Cu_2O). The study concluded that some of the intermediate phases such as Cu_4O_3 were unobservable because they are normally formed at the grain boundaries and hence cannot be confirmed by x-ray diffraction.

Trawiński & Kusz, (2021) also investigated the reduction of a mixture of bismuth, antimony and tellurium oxides (Bi_2O_3, Sb_2O_3 and TeO_2) in a hydrogen atmosphere for the synthesis of $BiSbTe_3$. It was revealed from the study that Sb_2O_4 reduced to Sb_2O_3 with the reaction commencing at 377 ºC. Above 557 ºC, further reduction of Sb_2O_3 led to the occurrence of elemental antimony (Sb). Similar processes were observed for the reduction of the mixture of antimony and tellurium oxide and a mixture of antimony and bismuth oxide. In the reduction process of both mixtures, hydrogen reduced the tellurium oxide to tellurium while the water formed oxidized the Sb_2O_3 to Sb_2O_4. Another interesting finding was that for the mixture of antimony and bismuth oxides, the two oxides influenced each other by decreasing the onset reduction temperature of antimony oxide and increasing the temperature for bismuth oxide. The result of the analysis of the mixture of the three oxides is similar to the mixture of the bismuth and tellurium oxide. The authors concluded that a generalized description of the reduction of the mixture of the three oxides is unavailable because the presence or absence of any of the oxides influences the overall reaction mechanism and by-products formed. The heating rate in the non-isothermal condition also influenced the process.

PARTIAL CONCLUSION

Detailed review of different aspects of the topic studied has been provided in this chapter. It has been observed from literature that hydrogen reduction process has been extensively explored especially in the reduction of iron oxide to iron. This is due to the continuous effort being put in place to decarbonize the steel industry. However, hydrogen reduction of tellurium oxide remains

under explored. The findings from this study will therefore add to the handful of knowledge on the hydrogen reduction of tellurium oxide to obtain metallic tellurium.

CHAPTER 2
MATERIAL AND METHODS

CHAPTER 2 MATERIAL AND METHODS

INTRODUCTION

In this chapter, the various materials, equipment and methods employed in the study for the realization of the objectives of the study are discussed. It should be noted that hydrogen reduction of tellurium oxide experimental trials were performed at RWTH Aachen University in Germany, specifically in the hydrometallurgical laboratory of the Institute of Process Metallurgy and Metal Recycling.

2.1 MATERIAL

The tellurium oxide (TeO_2) powder utilized for the hydrogen reduction experimental trials was purchased from Wuhan Tuocai Technology Company Limited. It has a purity level of up to 99.99 %, ensuring that all analysis and experiments performed on or with the powder produce true and relevant results with very minimal or no influence from other metals or impurities. Wuhan Tuocai Technology Company Limited is situated in China and focused on research, production and sales of materials and other compounds which are of high purity levels including tellurium oxide.

2.1.1 MATERIAL CHARACTERIZATION

In the study, the chemical composition of the tellurium oxide powder was analyzed in depth by inductively coupled plasma-optical emissions (ICP-OES). This was done to obtain more insight into the structure and to also confirm the purity of the powder material, possibly identifying any impurity phase.

The particle size of the tellurium oxide powder was also measured to gain understanding of the physical and chemical properties of the powder material. This is important as it can have repercussions on the reactivity and processing properties of the powder material.

Also Scanning Electron Microscopy (SEM) alongside Energy Dispersive Spectroscopy (EDS) was performed on some selected samples after experimental trials for the purpose of obtaining information on the phase composition and microstructure of the samples, analyzing the elemental composition of the samples and assessing the mechanism of the reduction reaction.

2.2 EXPERIMENTAL TRIAL SET-UP

Detailed assessment of the reduction reaction between hydrogen and tellurium oxide to produce metallic tellurium was performed using the rotary kiln furnace with a tube reactor.

2.2.1 ROTARY KILN (TUBE) FURNACE

The rotary kiln furnace used in the study as shown in the figure 2.1 below has a quartz kiln tube representing the setting where the reaction takes place (reactor vessel). The device is a laboratory scale module (TSO 1-11/400) manufactured by Carbolite Gero GmbH & Co. KG in Germany. It is equipped with heating elements and temperature sensors which are efficient and precise and allow the user or operator to set and maintain the required temperature needed for a particular process. The reactor vessel (quartz tube) in the device, however, does not rotate completely as in traditional rotary kilns but oscillates up to 314^{o} in each direction at a frequency between one and eight per minute (1-8/min). This oscillatory movement of the device allowed homogeneous heating of the sample treated, that is eliminating or minimizing temperature gradient and enhanced efficient mixing of the sample with the gas reactant, hydrogen in this case, thereby annihilating concentration differences. These key features of the selected rotary kiln (tube) furnace, in addition to its capability to simulate significant process changes including transfer of heat makes it suitable for adoption in the heat treatment of materials under controlled conditions.

Table 2.1: Summary of specifications of rotary kiln used in the study

Specification	Index
Maximum temperature (ºC)	1100
Number of heating zones	1
Reaction chamber dimensions (mm)	Ø 120 × 330
Reaction chamber capacity (ml)	620
Oscillation frequency per minute	1 to 8
Rotation in each direction	314º

Maximum power (W)	1860
Weight (kg)	88

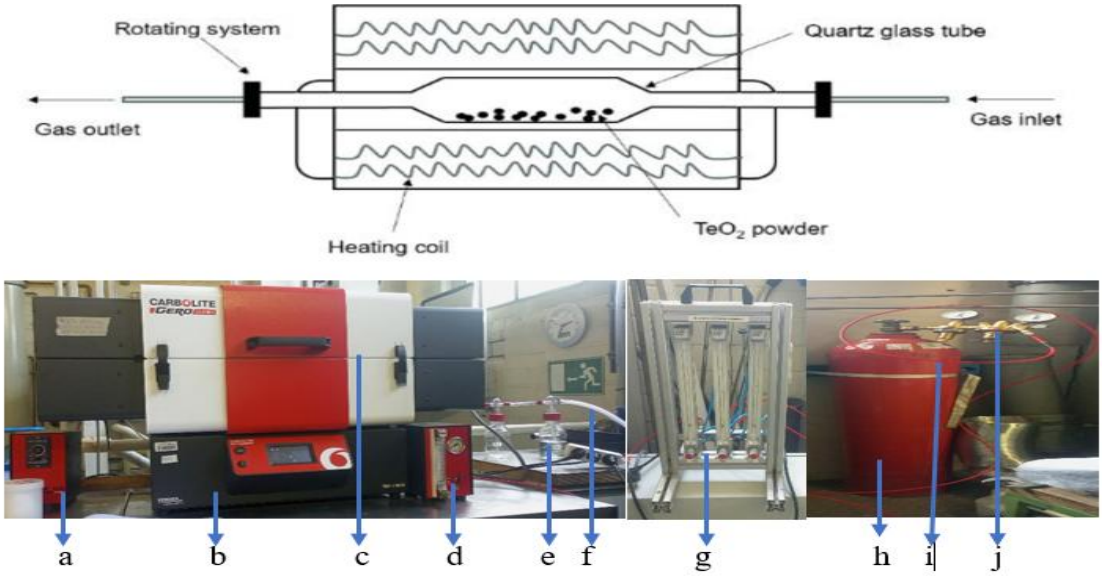

Figure 2.1: Schematic illustration of experimental set-up (top), experimental set-up of hydrogen reduction of tellurium oxide (bottom) with (a) rotation controller (b) control box (c) furnace body with quartz tube reactor (d) gas controller (e) distilled water bottle (f) output gas tube (g) gas mixture (h) hydrogen tank (i) gas pipe (j) pressure reducer

2.2.2 EXPERIMENTAL TRIAL PROCEDURE

The experiment started with the measurement of the mass of the empty quartz glass tube. Tellurium oxide powder was introduced into the empty quartz tube and this was weighed again. The mass of the empty quartz tube was then subtracted from the mass of the quartz tube containing the sample powder to obtain the initial mass of the powder (m_i) before the experiment. The tube containing the tellurium oxide powder was then fitted into the kiln device. Nitrogen gas was passed through the set-up to remove air and to check for any leakage in the set-up.

The required temperature and dwelling time were then set with the device put into operation by first heating the sample to the predetermined temperature. Hydrogen gas was then introduced into the set-up when the predetermined temperature was reached for the main reduction reaction to take place, as the predetermined temperature was held constant for the set dwelling time. When the dwelling time elapsed, the hydrogen supply was halted with occasional flushing of the system with

nitrogen gas to get rid of residual hydrogen. The system is allowed to cool to room temperature naturally and the quartz glass tube containing the residual sample was removed and weighed.

The final mass of the sample (m_f) after the experiment was then determined by subtracting the mass of the empty tube from the mass of the tube and residual sample after the experiment. The residual sample (reaction products) were then collected and sealed in a sample bag. It is also worth mentioning that gas leakage test was conducted as the reaction was taking place to prevent any unwanted escape and accumulation of hydrogen which is very dangerous.

A total of twenty-five (25) experiments were performed with varying temperatures, dwelling times and masses to ascertain the influence that each has on the reduction process of the tellurium oxide powder. The parameters are summarized in table 2.2 below.

Table 2.2: Experimental design and parameters

Experiment	Temperature (^{o}C)	Dwelling time (hours)
1	100	2
2		
3	200	
4		
5	300	
6		
7	430	
8		
9	600	
10		

11	100	3
12		
13	200	
14		
15	300	
16		
17	430	
18		
19	600	
20		
21	100	4
22	200	
23	300	
24	430	
25	600	

2.3 CALCULATIONS

2.3.1 REDUCTION RATE

The calculations of reduction rate for each trial experiment were done based on the mass loss of the tellurium oxide (TeO_2) used in each experiment, that is the difference in mass between the tellurium oxide sample before and after the experiment. This calculation is necessary as it gives

way to enhancing the experimental operations, yield and purity of the products at the end of the experiment.

The initial mass of the tellurium oxide sample before each experiment was measured and recorded as m_i while the corresponding final mass after the experiment was also measured and recorded as m_f. The mass loss (in percentage) of the tellurium oxide sample for each experiment was then calculated using the equation:

$$\text{mass loss} = \frac{m_i - m_f}{m_i} \times 100\% \tag{17}$$

This mass loss calculation is then compared to the theoretical mass loss (percentage) of oxygen in the tellurium oxide sample. This is because the oxygen content in the tellurium oxide represents the fraction of the solid sample effectively taking part in the chemical reaction specifically with the gaseous reactant, hydrogen to produce water. The theoretical mass loss or percentage of oxygen in the tellurium oxide sample is determined by comparing the molar masses of oxygen and the tellurium oxide sample and expressing it as a percentage. This was calculated from the equation below.

$$\text{mass loss}_{\text{theo}} = \frac{molar\ mass_{oxygen}}{molar\ mass_{tellurium\ oxide}} \times 100\% \tag{18}$$

Where $\text{mass loss}_{\text{theo}}$ is theoretical mass loss (percentage of oxygen in the tellurium oxide sample), $molar\ mass_{oxygen}$ represents the molar mass of oxygen and $molar\ mass_{tellurium\ oxide}$ represents the molar mass of tellurium oxide.

The reduction rate was then determined by comparing the mass loss calculated from the experiments and the theoretical mass loss, that is the percentage of oxygen content in the tellurium oxide and expressing it as a percentage. The calculations were done from the equation below.

$$\text{Reduction rate} = \frac{Experimental\ mass\ loss}{theoretical\ mass\ loss} \times 100\% \tag{19}$$

2.3.2 FLOW RATE OF HYDROGEN

The flow rate of hydrogen was determined by considering the overall reaction equation between tellurium oxide and oxygen shown below.

$$TeO_2 + 2H_2 \rightarrow Te + 2H_2O \quad (20)$$

The number of moles (n_1) of tellurium oxide was determined from the mole concept equation on mass bases as:

$$n_1 = \frac{mass_{TeO_2}}{molar\ mass_{TeO_2}} \quad (21)$$

The number of moles of hydrogen was then determined by multiplying the number of moles of tellurium oxide calculated by 2. This value was subsequently multiplied by 22.4 (volume of one mole of a gas at standard temperature and pressure) and 1.5 (over stoichiometry) to obtain the required volume of hydrogen needed for the reaction, including compensation for leakages and other inefficiencies. The required volume of hydrogen was then divided by the corresponding dwelling time of the experiment to obtain the flow rate of hydrogen during the experiment.

2.4 DETERMINATION OF REACTION KINETICS

To investigate the reaction kinetics of the chemical reaction between tellurium oxide and hydrogen, that is to determine kinetic parameters including the reaction model (mechanism) and activation energy, isothermal and non-isothermal differential thermal analysis and thermogravimetric analysis (DTA-TG) were carried out on the tellurium oxide powder in a hydrogen atmosphere in Fraunhofer IKTS. The DTA-TG analyses were performed at different temperature programs including 1, 2, 5 and 10 Kelvin/min (K/min).

This satisfies one of the recommendations of the kinetics committee of the International Confederation for Thermal Analysis and Calorimetry authored by (Vyazovkin et al., 2011). The study recommends that by using model fitting method, which is one of the methods employed in this study, results are reliable so far as different data sets obtained from thermal analysis performed under different temperature programs are simultaneously fitted into different models. In the DTA-TG analysis, the tellurium oxide sample was heated from around 15 ºC to 430 ºC at the respective heating rates stated above.

2.4.1 CHOOSING AN APPROPRIATE REACTION MODEL

To pick an appropriate reaction model, the data obtained from the isothermal DTA-TG analysis was evaluated by converting the mass loss into reaction extent or conversion. The data (conversion

and their corresponding time) were simultaneously fitted into some selected models shown in table 2.3 below, which have been used to typically model reactions between solids and gases, like the reactants considered in this study.

Table 2.3: Selected solid-gas reaction models used in the study

Model	Plot of linearity
Avrami-Erofeev	lnt versus $\ln(-\ln(1-\propto))$
Diffusion Shrinking Core	t versus $1-3(1-\propto)^{\frac{2}{3}}+2(1-\propto)$
Reaction Shrinking Core	t versus $1-(1-\propto)^{\frac{1}{3}}$
Jander	t versus $\left(1-(1-\propto)^{\frac{1}{3}}\right)^{2}$
Ginstling-Brounshtein	t versus $1-\frac{2\alpha}{3}-(1-\propto)^{\frac{2}{3}}$

A plot of linearity for each model was performed for data obtained from the different temperature programs and the best fit model was chosen as the model with the best linearity. The linearity was evaluated based on the coefficient of determination (R^2 value) for each plot of linearity. The model with the highest R^2 value for each plot of linearity under each temperature program was selected as the best fit model. The considerations for the development of the selected best fit model and the results obtained from the SEM-EDS analysis were combined to propose a mechanism for the reaction between tellurium oxide and hydrogen to produce metallic tellurium and water.

2.4.2 ESTIMATION OF ACTIVATION ENERGY OF THE PROCESS (MODEL FREE)

The data obtained from the non-isothermal analysis were evaluated by converting them to obtain reaction extent, reaction rate and other important parameters required for calculating the activation energy of the reaction. Three model free methods namely the Friedman, Flynn and Wall and or Ozawa (FWO) and Kissinger method were used to estimate the activation energies. The corresponding equations used for each method are shown in table 2.4 below.

Table 2.4: Model free methods and corresponding equations used for estimating activation energy

Model free method	Equation
Friedman	$\ln\left(\frac{d\propto}{dt}\right)_{\propto,i} = \ln[f(\propto)A_{\propto}] - \frac{E_a}{RT_{\propto,i}}$
Flynn and Wall and or Ozawa	$\ln(\beta i) = Const - 1.052\left(\frac{E_\alpha}{RT_\alpha}\right)$
Kissinger	$\ln\left[\frac{\beta}{T_{m,i}^2}\right] = \ln\left[-\frac{AR}{E}f'^{(\alpha_m)}\right] - \left(\frac{E}{RT_{m,i}}\right)$

For each method, the left-hand side of the equation was plotted against $\frac{1}{T_{\propto,m}}$ to obtain a straight line. The corresponding activation energies were calculated from the slope of the lines.

PARTIAL CONCLUSION

This chapter provided a description of the methods and equipment used for performing the experiment in the study. Characterization techniques used in the kinetic analysis were also outlined and highlighted.

CHAPTER 3
RESULTS AND DISCUSSION

CHAPTER 3 RESULTS AND DISCUSSION

INTRODUCTION

In this chapter, the results obtained from the various methods employed in the study are presented and discussed. The first part presents results and discussion of different characterization techniques including chemical composition, particle size analysis of samples, SED-EDS and DTA-TG analysis. This also included the interpretation of the DTA-TG data used in the modelled and model free kinetic analysis methods, with a proposed reaction mechanism for the hydrogen reduction of tellurium oxide to form metallic tellurium and water. The second part presents the results and discussion of further exploration of the process under varying conditions including temperature, time and mass.

3.1 MATERIAL CHARACTERIZATION

3.1.1 CHEMICAL COMPOSITION OF TELLURIUM OXIDE

The results of the chemical composition performed on the tellurium oxide sample powder by inductively coupled plasma-optical emissions (ICP-OES) are presented in table 3.1 below.

Table 3.1: Content of elemental impurity phases of tellurium oxide in part per million (ppm)

Ag	As	Bi	Cu	Fe	Ni	Pb	S	Sb	Zn
25.5	14.6	34.2	<1.00	7.99	<0.50	<0.50	4.36	n/A	0.74

The results shown in table 3.1 above from the chemical composition of tellurium oxide used in the study confirm that the oxide material contains some elemental impurities, however at low concentrations (in ppm levels). This makes the assumptions and other analysis performed on the sample powder highly reliable and with very little or no influence from other impurity materials.

3.1.2 PARTICLE SIZE DISTRIBUTION

The result of the measurement of the particle size distribution of the tellurium oxide powder used in this study is shown in figure 3.1 below with the particle size summary in table 3.2.

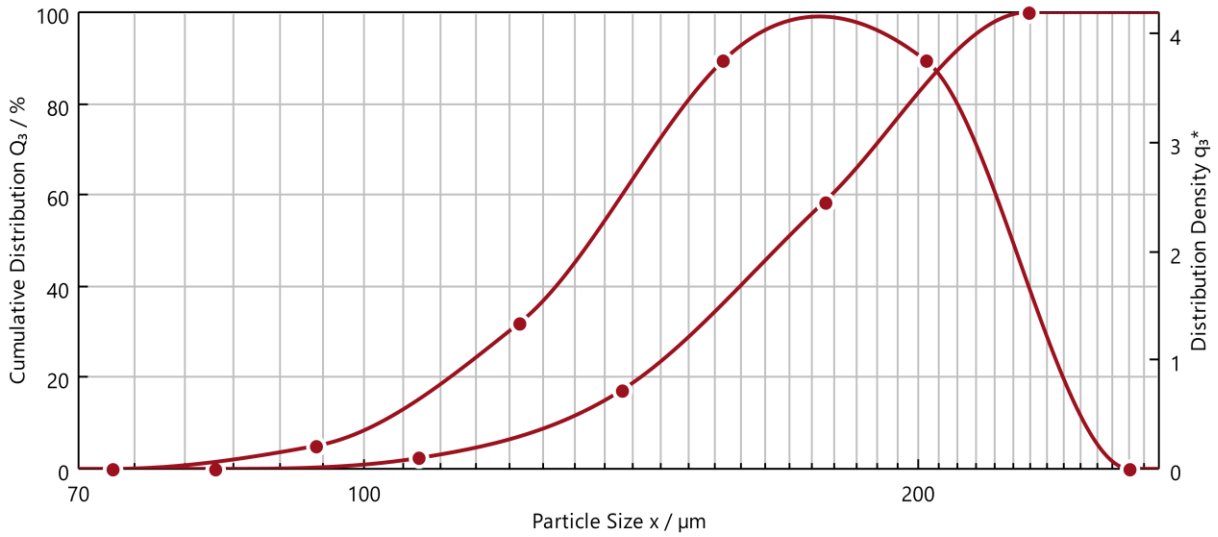

Figure 3.1: Particle size distribution of tellurium oxide powder

Table 3.2: Summary of particle size of tellurium oxide

Metric	Value (µm)
$X_{10.3}$	122.95
$X_{50.3}$	169.54
$X_{90.3}$	216.85
$X_{16.3}$	135.47
$X_{84.3}$	209.40
$X_{99.3}$	228.04
SMD	163.31
VMD	170.06
Particle count	11

The results from the particle size distribution of the tellurium oxide powder show that 10 % of the particles are smaller than a diameter of 122.95 µm while 90 % of the particles of the oxide are below 216. 85 µm. The surface mean diameter and volume mean diameter of the oxide particles were also measured to be 163.31 µm and 170.06 µm respectively and have a fairly spherical and irregular shape. In general, the particle size distribution is narrow with majority of the particles between 120 and 220 µm, displaying a profile which may influence diffusion rates and reactivity by enhancing the kinetics of the reduction process.

3.1.3 SEM-EDS ANALYSIS

Scanning Electron Microscopy alongside Energy Dispersive Spectroscopy (SEM-EDS) analysis performed on some of the samples after the experimental trial yielded results shown in figure 3.2 with percentage compositions of various spots in table 3.3 below.

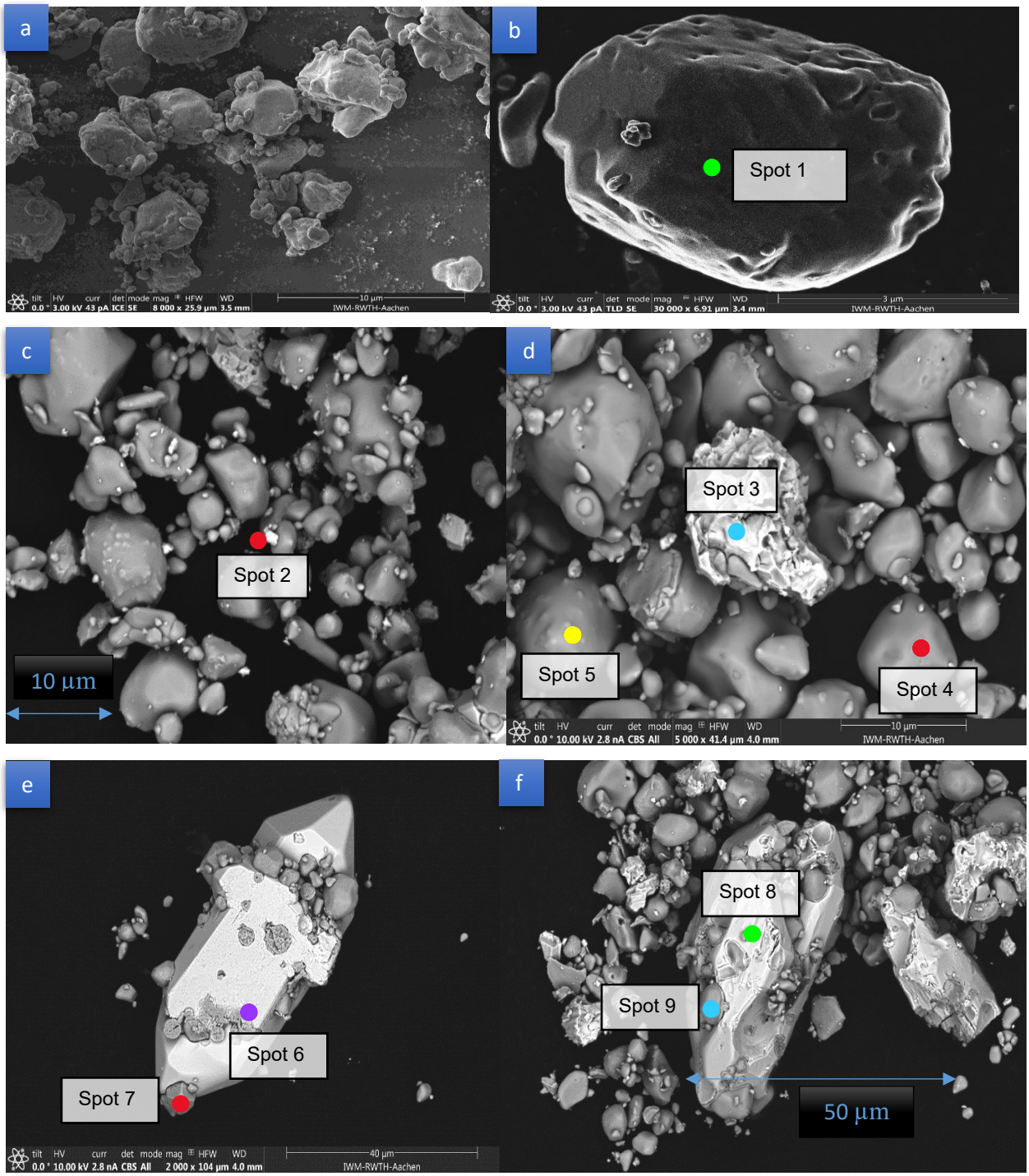

Figure 3.2: Images from SEM analysis on selected samples after experimental trials

Table 3.3: Percentage composition of various spots in SEM images

Spots	Te wt. %	O wt. %	Compound
1	82.1	16.3	$TeO_{1.56}$
2	> 99	-	Te
3	99.86	-	Te
4	83.27	16.53	$TeO_{1.58}$
5	84.92	15.08	$TeO_{1.42}$
6	99.89	-	Te
7	85.53	14.47	$TeO_{1.35}$
8	99.88	-	Te
9	85.31	14.69	$TeO_{1.37}$

From the SEM images observed above, it can be concluded and confirmed that the tellurium oxide particles have a somewhat elongated, spherical and irregular shape with coarse surfaces. The SEM images disclose noticeable metamorphosis in the particle structure of the samples confirming that the particles have undergone reduction by hydrogen. This is further confirmed by the elemental composition of the samples at various spots indicated on the images by the EDS analysis showing that both metallic tellurium and residual tellurium oxide phases coexist in the samples.

It can also be observed from the images, for instance in (b) that small metallic tellurium particles form on the surface of the tellurium oxide and these metallic tellurium particles separate from the oxide matrix, dispersing across the entire oxide surface with the oxide shrinking as the reaction proceeds. These small metallic tellurium particles can be observed as scattered shiny spots including spot 2 indicated in (c). Further observations at spot 3 in (d) also reveal that as the reaction progresses, the dispersed small metallic tellurium particles start attracting each other thereby

heaping together to form a cluster in the reaction setting while the oxide particles present, for instance as indicated at spots 4 and 5 continue to undergo reaction concurrently.

The metal cluster continues to grow larger by coalescing with surrounding metal particles. The cluster adopts a defined shape as it increases in size with some residual tellurium oxide particles adhering to its surface as shown in (e). The shape of the metal cluster becomes more defined as the adhered oxide particles are completely reduced, resulting in a well-structured and stable metal having a fine surface as indicated at spot 6 in (e). These interesting insights gathered from the observation of the SEM-EDS analysis images together with other methods were used to propose a reaction mechanism for the reaction between tellurium oxide and hydrogen gas to produce metallic tellurium and water.

3.2 RESULTS ON DETERMINATION OF REACTION KINETICS

3.2.1 DTA-TGA RESULTS

The results from the investigation of the thermal behavior of tellurium oxide under a hydrogen atmosphere using DTA-TG at different heating rates of 1, 2, 5 and 10 K/min is represented in figure 3.3 below, with temperature capping up to 430 ºC, followed by a ten hour (10 h) hold at that same temperature.

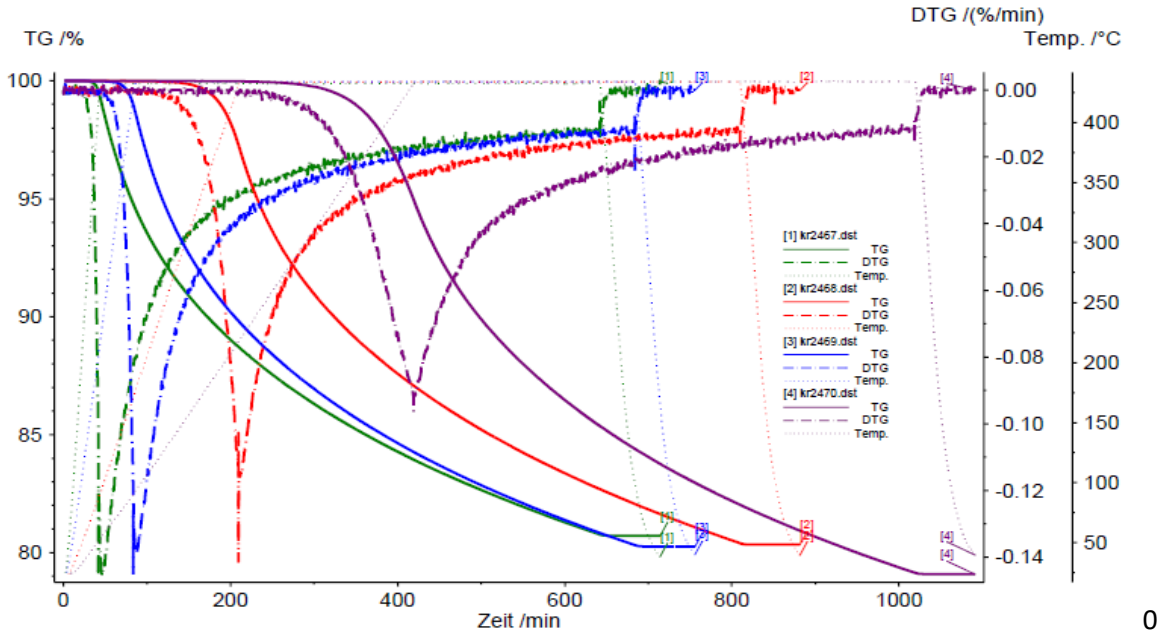

Figure 3.3: Mass change (TG) and mass change rate (DTG) of tellurium oxide as a function of time and characteristics temperatures under different heating rates (1, 2, 5 and 10 K/min)

The results from the thermal characteristics investigation of tellurium oxide reveal a one-step mass loss observed for all the heating rates, starting from 100 % and dropping steadily during heating, flattening at around 80 % with an overall mass loss of about twenty percent (20 %) as shown in figure 3.3 above by the TG curves. The 20 % mass loss aligns with the theoretical mass loss during reduction of tellurium oxide to metallic tellurium. The one step mass loss observation implies a single, continuous weight loss event experienced by the sample during heating as shown by the TG curves, indicating only one major reaction process occurred throughout the test. The mass loss was slightly greater at lower heating rates, possibly due to longer exposure and better interaction between the solid and the gas at lower heating rates. The mass loss in the investigation corresponds to the removal of oxygen atoms from TeO_2 as it reacts with hydrogen.

The DTG curves also reveal that faster heating rates caused sharper and quicker mass loss, with the rate of mass change dropping immediately the holding phase began at 430 ºC. This shows that most of the reduction occurred during heating of the sample, with no further mass loss observed after the 10 hours holding time and cooling of the sample. Slow or low heating rates on the other hand show smoother but slower mass loss, displaying a more gradual curve.

3.2.1.1 RESULTS OF COEFFICIENT OF DETERMINATION (R^2 VALUE) FROM THE PLOT OF LINEARITY OF SELECTED MODELS

The different coefficients of determination (R^2 values) calculated from the plot of linearity of the selected solid-gas reaction models for each heating rate after analyzing and fitting the DTA-TG data is shown in table 3.4 below.

Table 3.4: R^2 values obtained from the plot of linearity of selected reaction models.

MODELS	HEATING RATES/R^2 VALUES			
	10K/min	5K/min	2K/min	1K/min
Reaction Controlled Shrinking Core	0.9922	0.9929	0.9842	0.8175
Diffusion Controlled Shrinking Core	0.9863	0.9720	0.9380	0.8223
Avrami-Erofeev	0.8451	0.8998	0.9267	0.8861
Ginstling-Brounshtein	0.9863	0.9720	0.9380	0.8306
Jander	0.9436	0.8996	0.8619	0.5502

From the R^2 values shown in table 3.4, the Reaction Controlled Shrinking Core model consistently shows the highest values across most heating rates (2, 5 and 10 K/min), with values above 0.98 except at 1 K/min (0.8175). The Diffusion Controlled Shrinking Core and the Ginstling-Brounshtein models also show high coefficient of determination values, generally above 0.93 for most heating rates, despite being slightly lower than that of the Reaction-Controlled model. The Avrami-Erofeev model shows the highest value (0.8861) at 1 K/min. As evidenced by the highest overall R^2 values, especially at higher heating rates, the Reaction Controlled Shrinking Core model gives the best fit to the isothermal DTA-TG data.

However, since R^2 values statistically measure how well a fitted line explains the variation in data, the plots of linearity for most of the models (including the Reaction and Diffusion Controlled Shrinking Core model) explain more than 93 % of the variation in the data obtained from the DTA-TG analysis, especially at high heating rates. This implies that the models yielded comparably high R^2 values, indicating a possibility of multiple models being able to describe or fit the process.

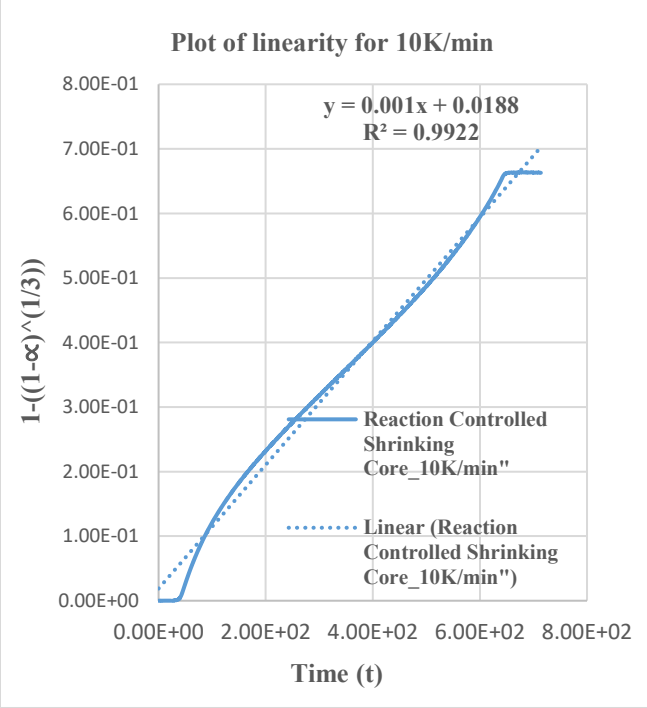

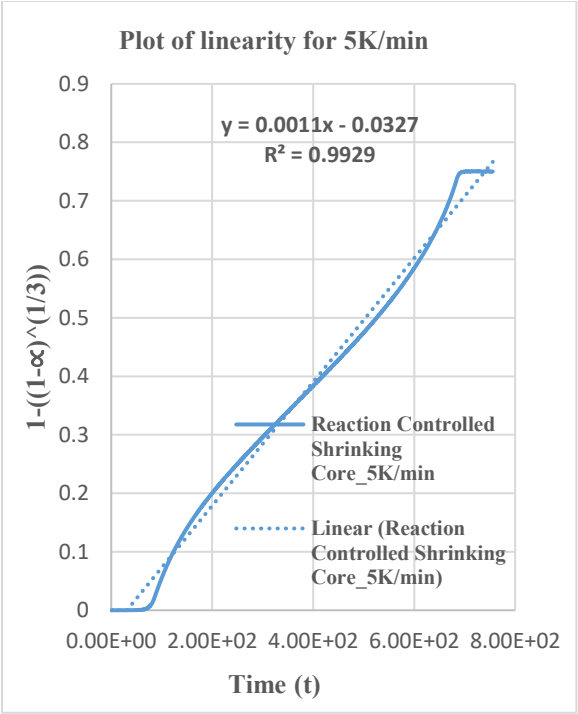

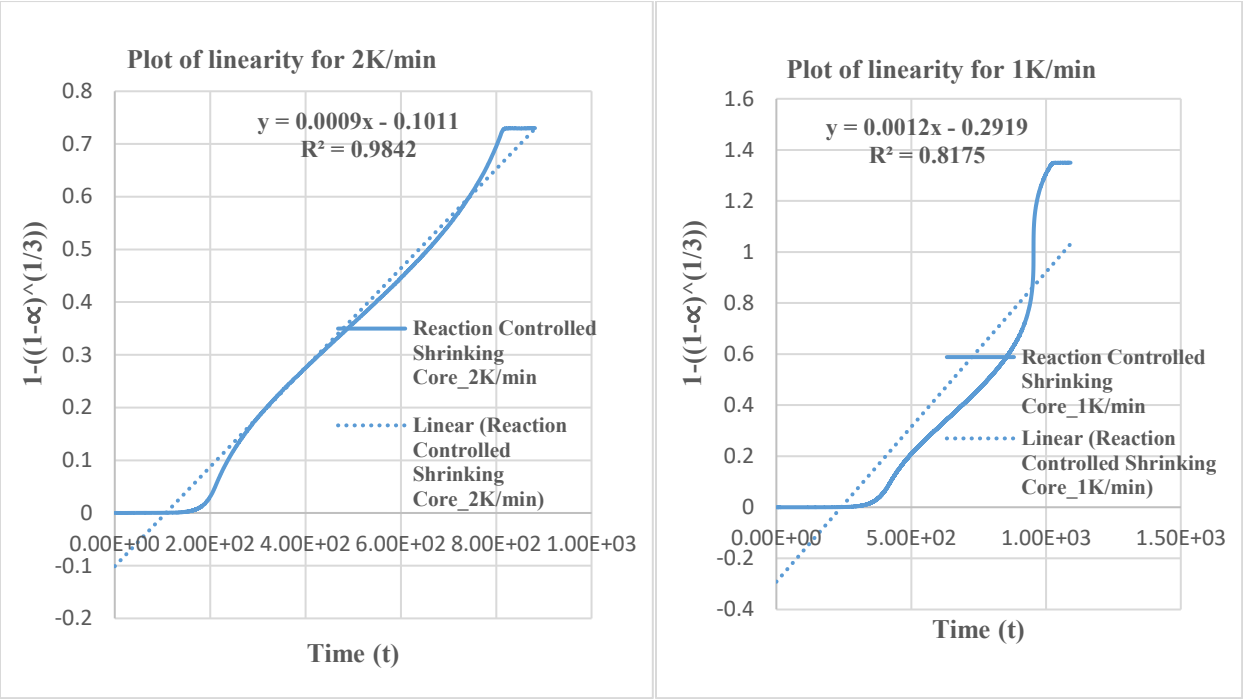

Figure 3.4: Plots of linearity for Reaction Controlled Shrinking Core Model

As most of the models have a high R^2 value, the process can be said to involve either a change or a combination of kinetic regimes. As such, other models also fit well with the data although the reaction controlled shrinking core model fits best. The conclusion drawn from the linear model fitting method of determining the mechanism of the reaction between tellurium oxide and hydrogen is that the reaction is likely to follow more than one reaction model including the reaction and diffusion controlled shrinking core models. Hence, the process can follow different reaction regimes throughout its entire conversion range. The considerations for the development of the shrinking core model in addition to observations and insights drawn from the SEM-EDS analysis as well as results from the model free methods were combined to propose a reaction mechanism between tellurium oxide and hydrogen gas to form metallic tellurium and water.

3.3 RESULTS FROM THE MODEL FREE METHODS

The basic data evaluated and collected for conversion (α) and corresponding temperature (T) from the non-isothermal thermogravimetric analysis of tellurium oxide under hydrogen atmosphere at different heating rates of 1, 5 10 and 20 K/min are shown in the table below. The data were collected for use in the model free methods.

Table 3.5: Conversion and temperature data at various heating rates for hydrogen reduction of tellurium oxide

Conversion (α)	Heating rate (β, K/min) / Temperature (°C)			
	1	5	10	20
0.1	385.57	449.96	473.65	504.99
0.2	417.41	471.47	498.20	535.61
0.3	439.85	485.13	515.18	555.10
0.4	450.34	496.09	528.84	572.08
0.5	454.94	505.79	541.15	588.73
0.6	459.10	515.71	554.11	603.00
0.7	464.08	525.85	567.67	615.30
0.8	471.78	540.20	585.72	612.84
0.9	487.25	561.56	606.86	602.00

According to the model free methods from equations (10), (14) and (16), a plot of $\ln\left(\frac{d\alpha}{dt}\right)$ against $\frac{1}{T}$ (Friedman), $\ln(\beta)$ against $\frac{1}{T}$ (Ozawa) and $\ln\left[\frac{\beta}{T^2}\right]$ against $\frac{1}{T}$ (Kissinger) for every conversion (α) from 0.1 to 0.9 yielded visuals in figure 3.5 shown below. The plots were performed for a wide range of conversion values (0.1 to 0.9) as recommended by (Vyazovkin et al., 2011). The activation energies for each conversion were then calculated from the slope of the lines ($\frac{E_\alpha}{R}$) and illustrated in table 3.6 below. The straight lines from the plots for each conversion (α) have a suitable linear correlation coefficient (R^2 value) with the slope of the lines in each plot changing as per the degree of the conversion value.

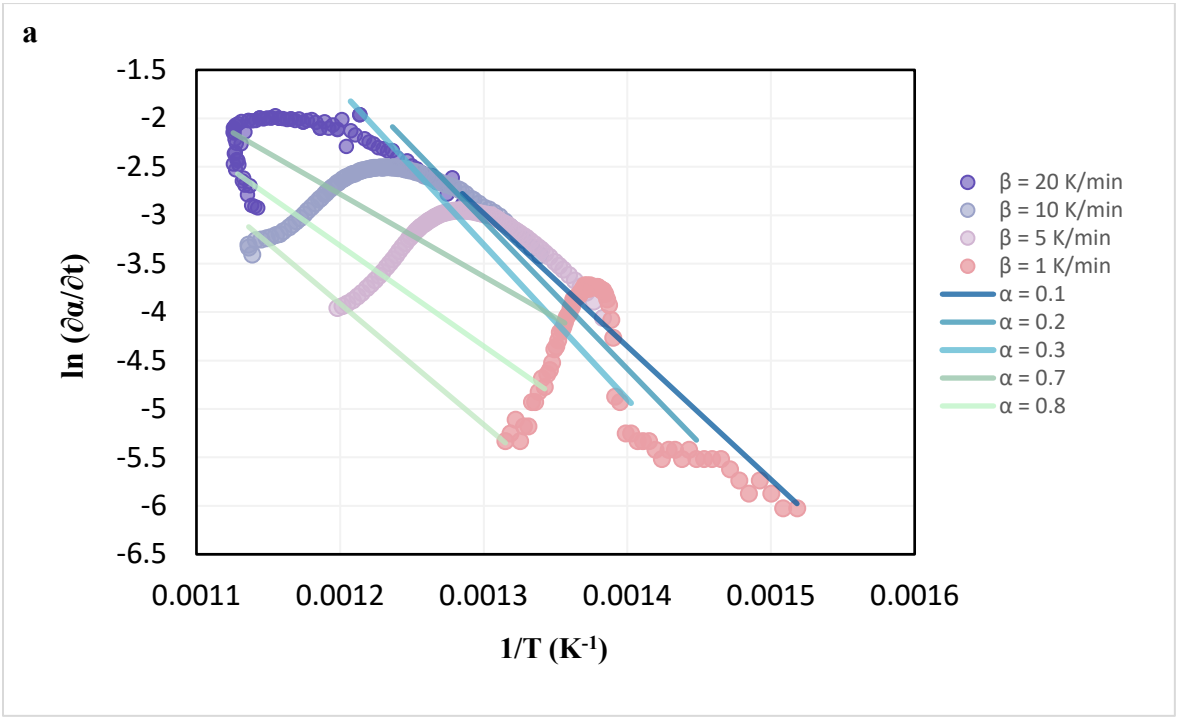
a
-1.5
-2
-2.5
-3
-3.5
-4
-4.5
-5
-5.5
-6
-6.5
ln (∂α/∂t)
0.0011
0.0012
0.0013
0.0014
0.0015
0.0016
1/T (K-1)
β = 20 K/min
β = 10 K/min
β = 5 K/min
β = 1 K/min
α = 0.1
α = 0.2
α = 0.3
α = 0.7
α = 0.8

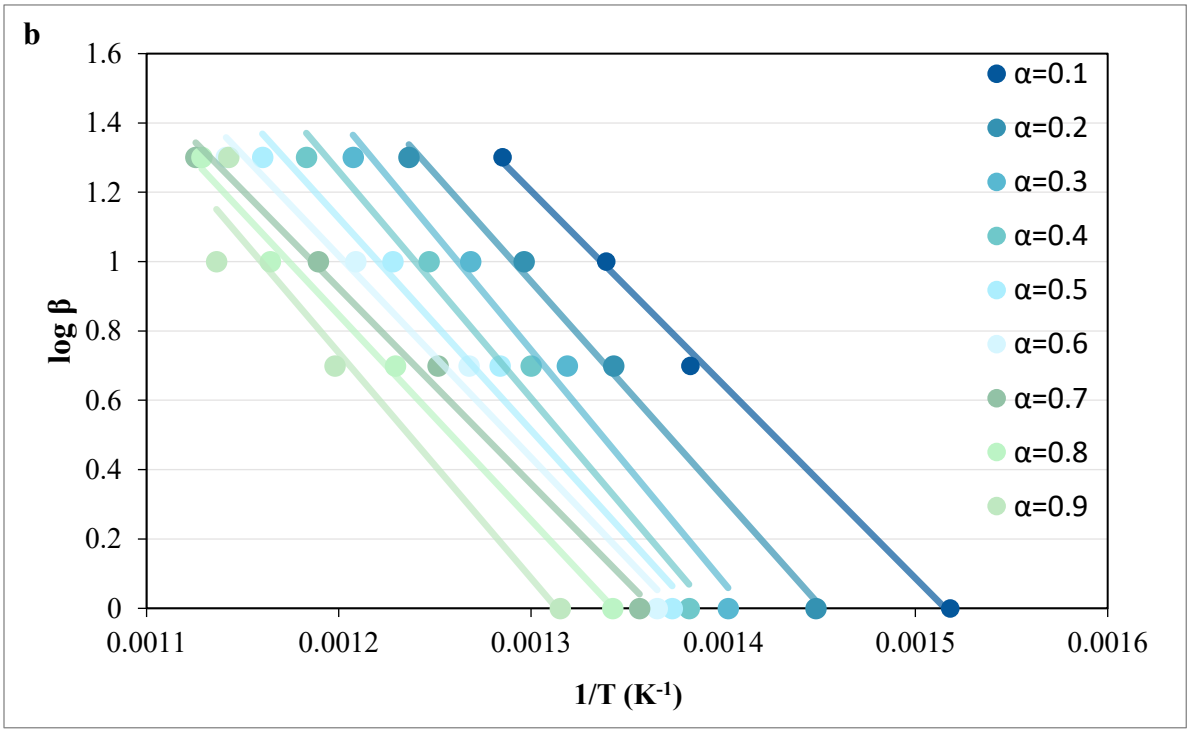
b
1.6
1.4
1.2
1
0.8
0.6
0.4
0.2
0
log β
0.0011
0.0012
0.0013
0.0014
0.0015
0.0016
1/T (K-1)
α=0.1
α=0.2
α=0.3
α=0.4
α=0.5
α=0.6
α=0.7
α=0.8
α=0.9

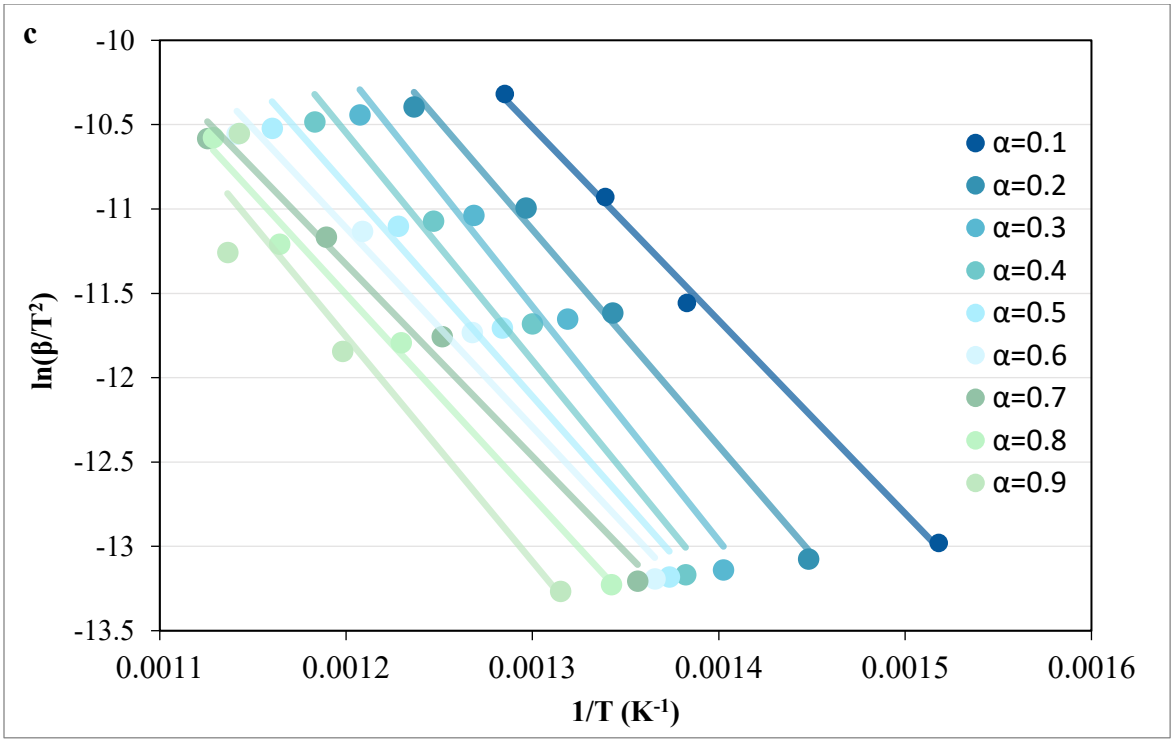

Figure 3.5: Friedman analysis (a), Ozawa analysis (b) and Kissinger analysis (c) for hydrogen reduction of tellurium oxide

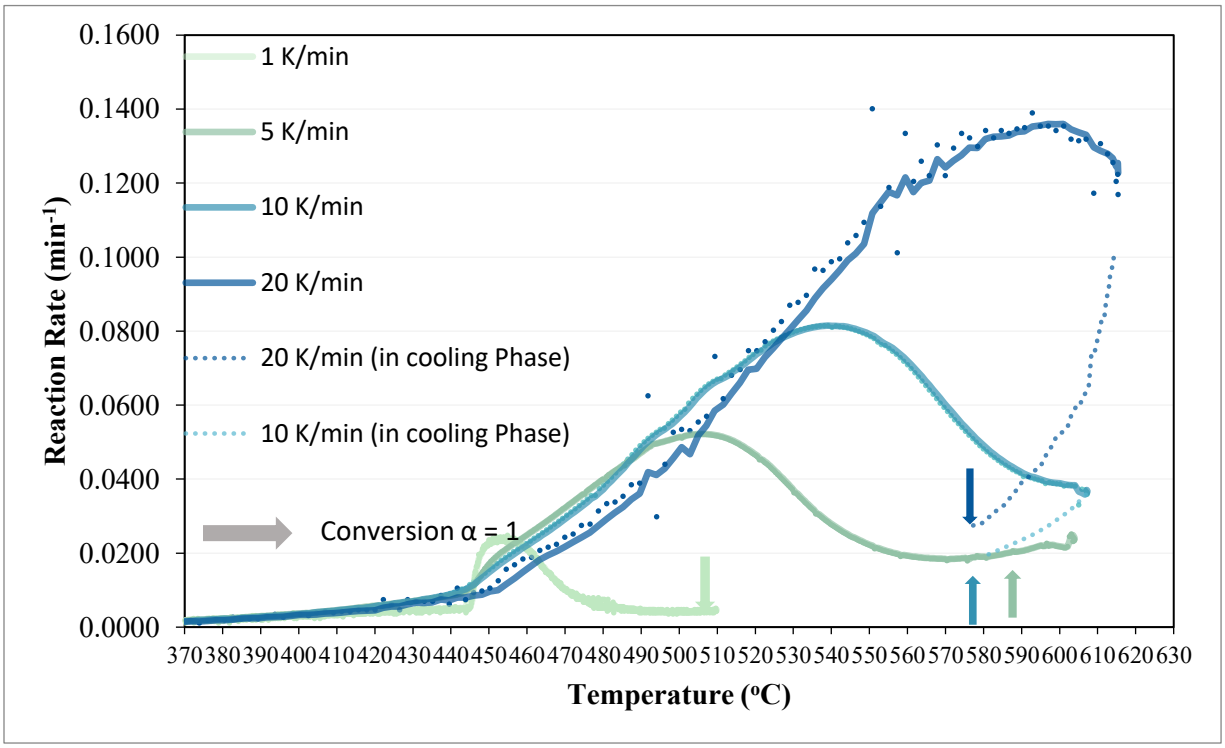

Figure 3.6: Reaction rate curve of non-isothermal thermogravimetric analysis of tellurium oxide under hydrogen atmosphere at different heating rates

It can be observed from table 3.6 that the calculated activation energies for each conversion (α) by the Friedman method vary significantly with each other, implying that the activation energy of the process depends on the conversion. However, values obtained by the Ozawa and Kissinger methods show very low variation as these methods usually produce single values of activation energy regardless of the kinetic complexity of a process (Fedunik-Hofman et al., 2019; Vyazovkin et al., 2011). An insignificant or a slight variation of the activation energies would have meant that the activation energy of the process is independent of the conversion, hence the process may be a simple reaction.

Table 3.6: Calculated activation energies and coefficients of correlation (R^2) for each conversion by the model free methods

Conversion (α)	Friedman method		Ozawa method		Kissinger method	
	E_a (kJ/mol)	R^2	E_a (kJ/mol)	R^2	E_a (kJ/mol)	R^2
0.1	114.22	0.99474	101.72	0.99748	107	0.99765
0.2	127.04	0.96266	113.21	0.99613	119	0.99564
0.3	132.68	0.92217	121.85	0.98299	128	0.98204
0.4	72.61	0.99712	119.03	0.97816	125	0.97710
0.5	65.78	0.99961	111.36	0.98040	117	0.97938
0.6	66.63	0.99941	105.94	0.98606	111	0.98521
0.7	70.69	0.99421	102.69	0.99126	108	0.99063
0.8	86.30	0.98150	107.72	0.99450	113	0.99481
0.9	103.73	0.96213	118.34	0.93337	124	0.93520
Average	**93.30 ± 26.68**	**0.97939**	**111.32 ± 7.35**	**0.96877**	**116.89 ± 7.67**	**0.97275**

As such, it is imperative to employ an iso-conversional method to confirm the accuracy of values determined by the Kissinger method (Vyazovkin et al., 2011). The use of the Ozawa method to

back up estimates from the Kissinger method is discouraged as such practices only reveal trivial difference in the activation energy values. This is because the two methods are as a result of approximations of different accuracies made on the same equation (Vyazovkin et al., 2011). The Friedman method is therefore used as back up to the Kissinger estimates in this study. The Friedman method, unlike the Kissinger and Ozawa methods is universal as it can be applied to a wide variety of temperature programs. The Kissinger and Ozawa methods are limited to linear heating rate conditions. Furthermore, the introduction of approximations in the Kissinger and Ozawa methods mean that the Friedman method is potentially more accurate (Fedunik-Hofman et al., 2019).

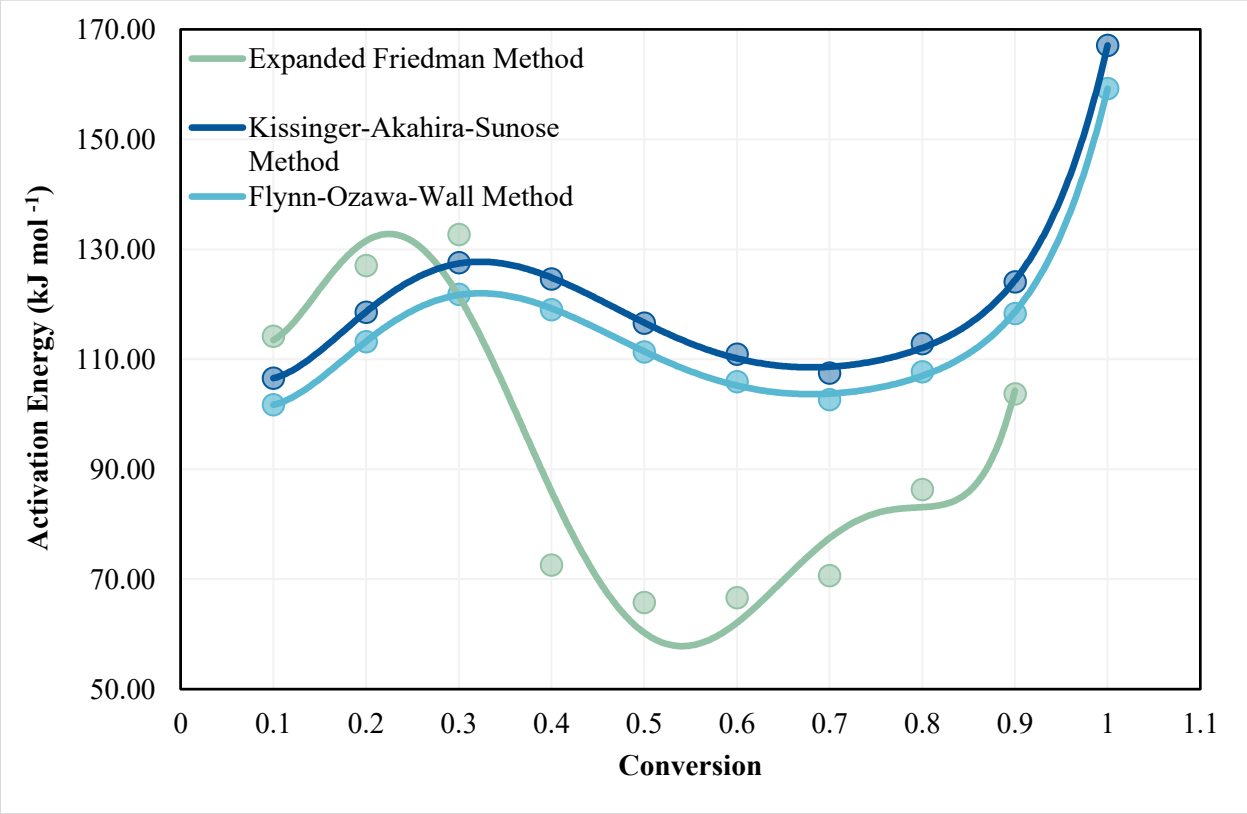

Figure 3.7: Trend of calculated activation energies for each conversion by the model free methods

It is clear from the calculated activation energy values by the Friedman method, having a mean of approximately 93.30 ± 26.68 and a coefficient of variation of about 29 % that the values do not back the Kissinger estimates. This signifies that the spread of the activation energy values is large with reference to the mean. Since a coefficient of variation above 20 % is usually considered to imply a significant variation in most contexts, the calculated activation energy values by the

Friedman method can then be said to vary significantly from each other. However, the mean Friedman value is closer to values obtained for the hydrogen reduction of lead oxide reported by Ivanov et al., (2015) to be between 85.8 and 93.1 kJ/mol. Even though the Friedman method is also a model free method, it can give a mechanistic clue of a process based on activation energy dependence on conversion or degree of variation of activation energy with conversion (Vyazovkin et al., 2011).

A substantial change in activation energy with conversion implies that a process is kinetically complex, indicating a change from one mechanism to another during the process. As such, since the calculated activation energies for the process studied in this work vary significantly with each other, it is concluded that the hydrogen reduction of tellurium oxide could be a multi kinetic mechanism. This implies that applying a simple step mechanism to describe the kinetics of the entire range of experimental conversions and temperature of the process is impossible. This conclusion also corresponds to the multiple peaks observed in the reaction rate curves of the process at different heating rates (1, 5, 10 and 20 K/min) in figure 3.6 as well as the undulating (increasing and decreasing) nature of the activation energies of the process illustrated in figure 3.7.

3.4 PROPOSED REACTION MECHANISM

The reaction mechanism proposed in the study for the solid-gas reaction between hydrogen (H_2) and tellurium oxide (TeO_2) to form metallic tellurium (Te) and water (H_2O) is a multi-kinetic mechanism with no intermediate particle or material formed during the process. The mechanism is based on results obtained from kinetic analysis and scanning electron microscopy and energy dispersive spectroscopy (SEM-EDS) observations made on some experimental trial residues. The kinetic analysis involved both the modelled and model-free methods, using kinetic data obtained from isothermal and non-isothermal differential thermal and thermogravimetric analysis (DTA-TGA) respectively. The modelled method suggests a possible fit of the reaction for more than one reaction model including the reaction and diffusion controlled shrinking core models. The model-free method complemented results from the modelled method by implying that the reaction involves multiple kinetic regimes.

As such, the multi-step process of the studied reaction begins with an external mass transfer involving the diffusion of the gaseous reactant, hydrogen (H_2) from its bulk phase to the surface

of the solid reactant, tellurium oxide. The hydrogen molecule, the adsorbate, then get adsorbed (adheres without penetrating) onto the surface of the tellurium oxide particle, the adsorbent. This initial process may depend on how fast the hydrogen is able to diffuse through as well as get adsorbed onto the tellurium oxide particles before a reaction can occur. The process suggests diffusion of hydrogen as the rate limiting step. The competitive R^2 values for the diffusion-controlled models indicate the importance of diffusion in this kinetic regime.

This is then followed by a surface reaction between the adsorbed hydrogen molecules and the tellurium oxide particles. Here, the progress of the entire reaction process may switch from diffusion controlled to surface reaction controlled as more hydrogen get adsorbed to the surface of the oxide particles. The high R^2 values for the reaction controlled shrinking core model supports this kinetic regime. With the tellurium oxide particle assumed to be a non-porous and an irregularly shaped core, the reaction between hydrogen and the oxide should leave behind a product layer (tellurium) around the unreacted core (tellurium oxide) as the reaction proceeds. This is in accordance with the mechanism of a shrinking core model. However, sample analysis from SEM-EDS reveals the separation of the product layer (tellurium) from the oxide matrix with the oxide shrinking.

As the reaction proceeds, more elemental tellurium is formed which get dispersed within the reaction environment. This residual build up may hinder the further diffusion and adsorption of hydrogen as well as desorption of water from the reaction surface for further reaction to occur. As such, both the reaction and diffusion-controlled regimes may operate simultaneously or switch from one to the other depending on the conditions of the experiment. The non-monotonic trend of the activation energy observed in figure 3.7 supports this suggested overlap between the two kinetic regimes. Since this is a redox reaction, the half and overall equations at the reaction surface are shown in equations (22), (23) and (24) below. During the reaction, hydrogen is oxidized (loses electrons) and in the presence of oxygen in tellurium oxide, forms water while tellurium in tellurium oxide is reduced (gains electrons) to elemental tellurium. The overall reaction is obtained by combining both equations and balancing the electrons involved in the reactions.

$$H_{2(g)} \rightarrow 2H^{+}_{(g)} + 2e^{-} \text{ (oxidation)} \quad (22)$$

$$TeO_{2(s)} + 4H^{+}_{(g)} + 4e^{-} \rightarrow Te_{(s)} + 2H_2O_{(g)} \text{ (reduction)} \quad (23)$$

$$TeO_{2(s)} + H_{2(g)} \rightarrow Te_{(s)} + 2H_2O_{(g)} \text{ (overall reaction)} \quad (24)$$

The reaction proceeds as water desorbs from the reaction surface in the form of vapor due to surrounding temperatures while elemental tellurium formed heaps together to form a cluster. This transformation suggests a possible nucleation and growth dynamics during initial tellurium formation. The entire process may then be limited by another kinetic regime, the nucleation and growth of the elemental tellurium, towards the end of the reaction. This regime is supported by the moderate fits of the Avrami-Erofeev model. Unreacted tellurium oxide particles, due to their nature, may also agglomerate and get attached to the cluster of tellurium metal formed. The process continues until the reduction is complete or incomplete depending on the temperature and dwelling time. The entire process features sequential or simultaneous overlapping of different kinetic regimes, beginning as a diffusion limited process. It then transitions into a surface reaction-controlled process and then to a simultaneous overlap of both kinetic regimes midway. Towards the end, the process becomes limited by the nucleation and growth of elemental tellurium formed. This mechanistic complexity of the process is common in solid gas reduction processes and it is justified by the modelled and model free methods employed in the kinetic analysis in this study.

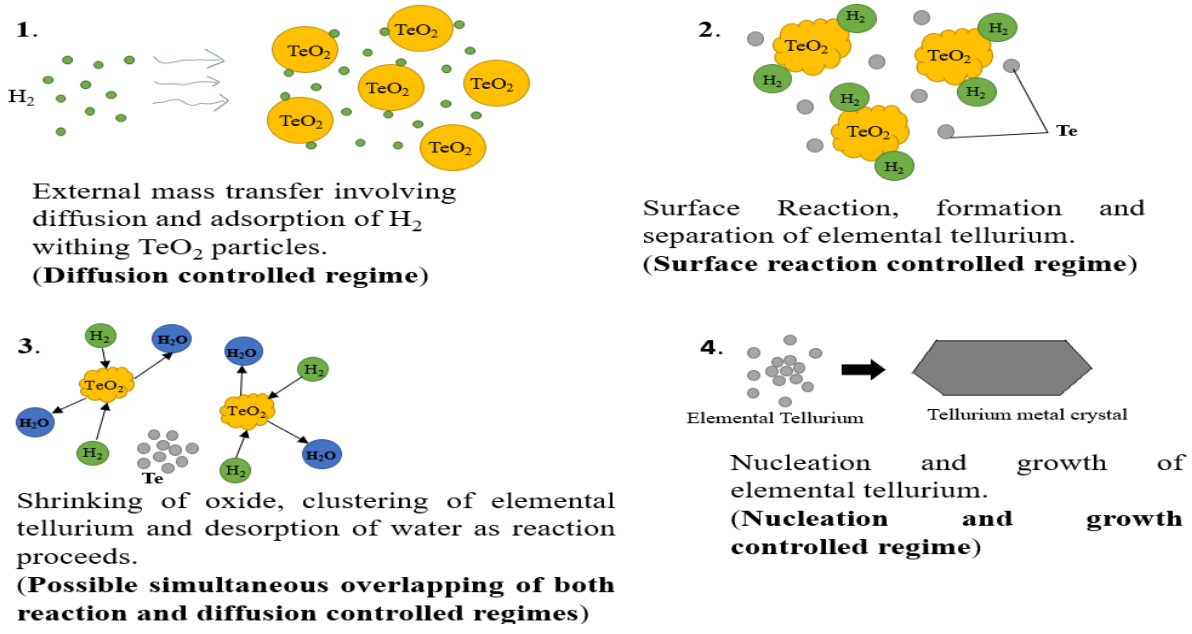

Figure 3.8: Proposed reaction mechanism of hydrogen reduction of tellurium oxide.

3.5 EXPERIMENTAL TRIAL RESULTS FROM ROTARY KILN

The results of the reduction rates for the twenty-five (25) set of experiments conducted in the rotary kiln were calculated using the equations presented in Chapter 2 (equations (17) and (19)). These

experiments were conducted under varying conditions including temperature, mass and time. Table 3.7 below shows a summary of each condition alongside the corresponding reduction rate.

Table 3.7: Reduction rate of experimental trials from rotary kiln for each varying condition

Experiment	Temperature	Dwelling time	Reduction rate
1	100	2	1.499
2	100	2	1.005
3	200	2	1.114
4	200	2	2.174
5	300	2	5.609
6	300	2	6.126
7	430	2	48.028
8	430	2	29.096
9	600	2	102.124
10	600	2	89.442
11	100	3	0.815
12	100	3	0.979
13	200	3	3.271
14	200	3	2.634
15	300	3	5.240
16	300	3	6.234

17	430	3	43.979
18	430	3	42.461
19	600	3	66.958
20	600	3	103.336
21	100	4	1.620
22	200	4	4.783
23	300	4	7.243
24	430	4	57.726
25	600	4	108.552

The results above, obtained from the calculation of reduction rate of each experiment were analyzed to assess the effect of the varying conditions on the reduction rates. This was done through figures. A general overview of the results however shows lesser reduction rates at lower temperatures between 100 and 300 ^{o}C and a drastic increase in the reduction rate from a temperature of 430 ^{o}C and above.

3.5.1 EFFECT OF VARYING MASS ON THE REDUCTION RATE

To assess the effect of varying the mass of the tellurium oxide sample used in the experimental trial on the rate of reduction, different masses were used for the experimental trials with the two hours (2 h) dwelling time. The masses ranged from 100 g to 277 g. Figure 3.9 below shows a graph of the reduction rate for the two-hour dwelling time experiments under different temperature conditions and mass of sample used.

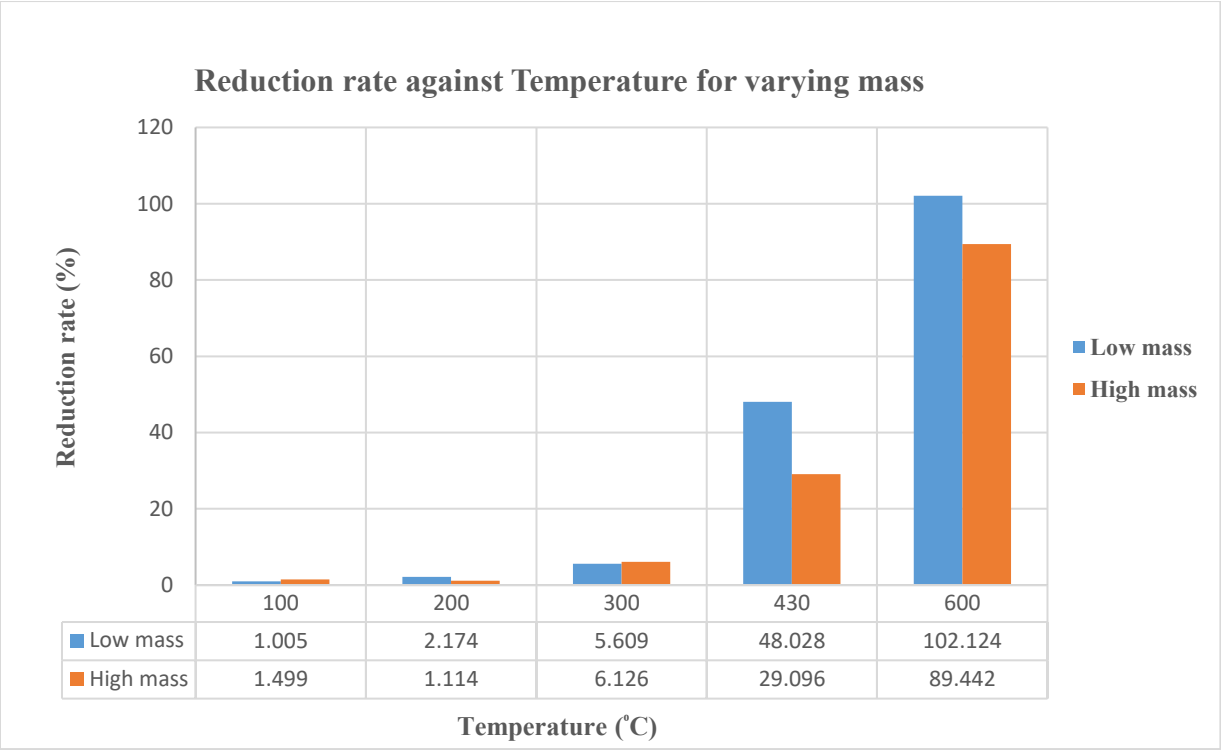

Figure 3.9: Reduction rate against temperature for different masses with two-hour dwelling time

It can be observed from the figure 3.9 above that the reduction rate decreases with high mass and vice versa with low mass. This is clearly visible, especially for temperatures of 430 °C and above. The high yield of reduction rate for low masses could possibly be attributed to the fact that the oxide sample due to its quantity at a given temperature and time was able to mix thoroughly with the gaseous reactant thereby enhancing the tendency for the reduction process to take place. Conversely, the mixing efficiency of the samples with high masses was lower compared to those with low masses, hence, leading to a lower yield in reduction rate compared to those with low masses.

To this effect, the reaction chamber of the rotary kiln should be filled between 3 to 6 % of its capacity (Volume bases) at operation condition of 430 °C and two-hour dwelling time if a reduction rate of about 30 to 50 % is required. However, at an operation condition of 600 °C and two-hour dwelling time, the capacity of the reaction chamber should be filled between 5 to 8 % if a reduction rate of about 90 to 100 % is required. This implies that to achieve a complete reduction when operating the rotary kiln at 600 °C and two-hour dwelling time, its reaction chamber should not be filled by more than 5 % of its capacity.

Reverse observations can be seen for temperatures at 100 and 300 °C as high masses yielded slightly higher reduction rates compared to low masses. Experiments at these temperatures including 200 °C were performed at continuous flow of hydrogen for low mass and interval flow for high mass as compared to those at 430 and 600 °C which were performed at continuous flow for both high and low masses. As such, the variation of the hydrogen flow could lead to the reverse observations at 100 and 300 °C, suggesting that interval flow of hydrogen results in a better reduction rate compared to continuous flow. However, this is beyond the scope of this research and needs to be verified.

3.5.2 EFFECT OF VARYING TEMPERATURE AND TIME ON REDUCTION RATE

The influence of temperature and dwelling time on the hydrogen reduction of tellurium oxide was assessed by running experiments under varying temperature conditions (100, 200, 300, 430 and 600 °C) and time (3 and 4 hours) with similar sample masses of about 150 g. Figure 3.10 depicts the dependence of the reduction rate on the temperature and dwelling time.

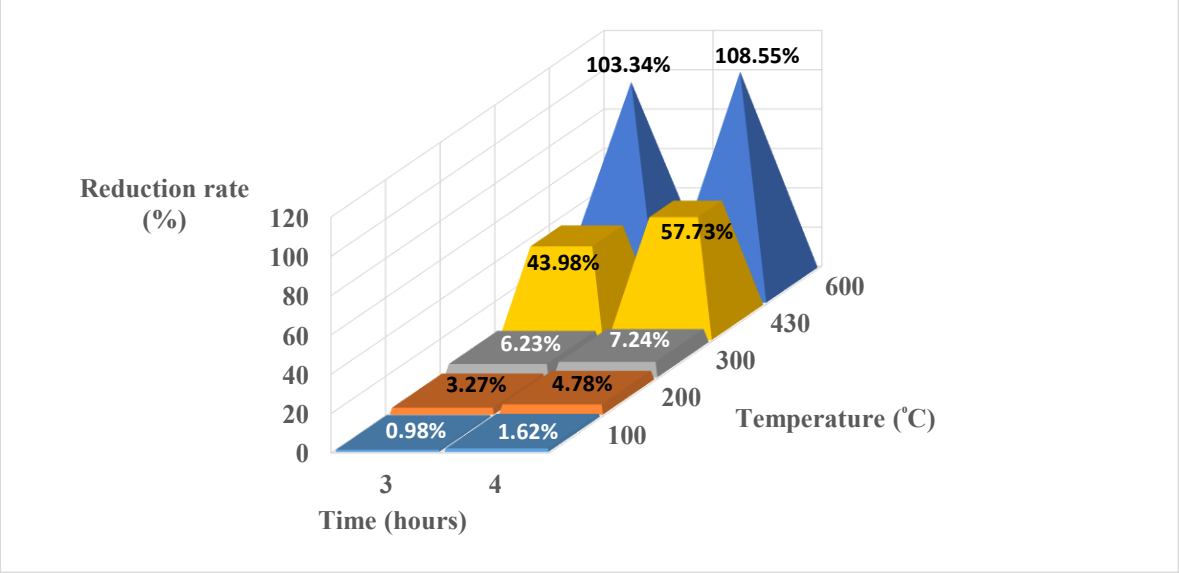

Figure 3.10: Reduction rate against temperature and dwelling time.

As observed in figure 3.10, the hydrogen reduction of tellurium oxide is possible at temperatures below the melting point of tellurium (449.8 °C). Generally, increase in reaction temperature has a direct variation on the reduction rate. The variation in the reduction rate is however small at temperatures below the melting point of tellurium between 100 and 300 °C. At temperatures closer to or higher than the melting point of tellurium, the reduction rate is observed to increase

substantially. This implies that even though the reaction is spontaneous below the melting point of tellurium, increase in reaction temperature increases the kinetics of the reaction.

The substantial increase in reduction rate from 430 °C is because at higher temperatures (430 °C and above), the average kinetic energy of the reactants (hydrogen and tellurium oxide) increases. As such, larger portion of the reactants possess kinetic energy either equal to or higher than the activation energy of the reaction. This leads to an increase in successful collisions among reactants leading to the formation of products. At 600 °C, a complete reduction of tellurium oxide was achieved. Since this temperature is higher than the melting point of tellurium, any elemental tellurium produced during this reaction temperature remained in molten form. As such, the interaction between unreacted tellurium oxide particles and hydrogen gas intensified as the adhesion between the molten tellurium and unreacted oxide reduced, leading to a complete reduction.

The estimated reduction rates at 600 °C exceeded 100 %. This is due to the evaporation of the product metal which remained in the molten state during the reduction process. As such, the measured mass loss may include small portions of the evaporated tellurium metal which by means of water vapour or the reducing gas, transported out of the kiln reactor. The evaporated metal, possibly could also adhere to either oxide or metal particles in the glass tube reactor, a phenomenon which is likely to happen as the setup for the experimental trials allows only gas to exit the tube reactor as highlighted by Chung *et al.,* (2025).

The influence of dwelling time on the reduction rate also followed an increasing trend, however, not as pronouncing as temperature. The only significant variation in the reduction rate, influenced by the dwelling time was observed at 430 ºC, where a 3-hour dwelling time yielded a rate of 43.98 % as against 57.73 % for a 4-hour dwelling time, representing an increase of about 14 %. In Chung *et al.,* (2025), where extended dwelling times of up to 7 hours were studied, significant variations in the reduction rate were observed at lower temperatures between 200 and 300 ºC. In the said study, the authors recorded an increase in reduction rate of about 12 % at 300 ºC between a 2 and 5-hour dwelling time and an increase of almost 17 % at 200 ºC between a 2 and 4-hour dwelling time. These extended dwelling times are, however, beyond the scope of this assessment as only 3 and 4-hour dwelling times were considered.

PARTIAL CONCLUSION

The hydrogen reduction of tellurium oxide is controlled more by kinetics than thermodynamics. Increase in reaction temperature (between 430 and 600 ºC) has more significance in the reduction rate of the process than increase in dwelling time and mass. The entire reaction process is multi-mechanistic featuring various rate limiting steps including diffusion, surface reaction and nucleation and growth of metal crystals.

GENERAL CONCLUSIONS AND PERSPECTIVES

GENERAL CONCLUSIONS AND PERSPECTIVES

In this study, the hydrogen reduction of tellurium oxide has been characterized through kinetic analysis and experimental data. The kinetic analysis involved both modelled and model free methods using data obtained from isothermal and non-isothermal differential thermal and thermogravimetric analysis respectively. The experimental data, involving the reduction rates of the process, were obtained through a further exploration of the reduction process at varying experimental conditions including temperature, time and mass. From the findings of the study, it has been concluded that:

- ✓ The hydrogen reduction of tellurium oxide is a multi-step process with no intermediate product formed during the process.
- ✓ The reduction process is mechanistically complex, indicating a change from one mechanism to another during the process.
- ✓ The whole reduction process involves a sequential or simultaneous overlapping of various kinetic regimes, possibly starting with a diffusion-controlled regime and then transitions into a reaction-controlled process. Midway through the reaction, a simultaneous overlap of both kinetic regimes is possible while nucleation and growth of elemental tellurium formed becomes the rate limiting step towards the end of the process.
- ✓ Hydrogen reduction of tellurium oxide is possible below the melting point of tellurium with increase in temperature between 430 and 600 ºC having a significant influence on the kinetics of the reaction more so than the dwelling time.
- ✓ The reduction process is feasible in a rotary kiln with a higher reduction rate for a low mass of sample compared to a high mass of sample.

At the end of this work, the following perspectives can be made:

- ➢ Further exploration of the hydrogen reduction of tellurium oxide should involve the use of different sample (tellurium oxide) types being sintered or nano-powder to ascertain the reactivity of each sample type.
- ➢ The reduction experiments should be interrupted at intervals and samples analyzed to investigate the possibility of obtaining intermediate products such as in the reduction of iron oxide to iron.

- The flow of the reducing gas (hydrogen), being continuous or at intervals, should be investigated to determine which flow type has more influence of the reduction rate of tellurium oxide.
- The reaction mechanism proposed in the study should be verified by other means such as the combined kinetic analysis method.

BIBLIOGRAPHIC REFERENCES

Atmaca, A., & Yumrutaş, R. (2014). Analysis of the parameters affecting energy consumption of a rotary kiln in cement industry. *Applied Thermal Engineering*, *66*(1–2), 435–444. https://doi.org/10.1016/j.applthermaleng.2014.02.038

AZoM. (2011). Tellurium Dioxide (TeO2) – Properties and Applications. *AHP Materials, Inc*. Accessed on June 02, 2025 from https://www.azom.com/article.aspx?ArticleID=5817

Ba, L. A., Döring, M., Jamier, V., & Jacob, C. (2010). Tellurium: An Element With Great Biological Potency and Potential. *Organic and Biomolecular Chemistry*, *8*(19), 4203–4216. https://doi.org/10.1039/c0ob00086h

Behera, S. K., & Sukla, L. B. (2012). Kinetics study for lateritic Chromite overburden leaching by organic (oxalic) acid. *Elixir Online Journal*, *Pollution 53*, 11890–11893. Accessed on May 25, 2025 from www.elixirjournal.org

Bojanovský, J., Máša, V., Hudák, I., Skryja, P., & Hopjan, J. (2022). Rotary Kiln, a Unit on the Border of the Process and Energy Industry—Current State and Perspectives. *Sustainability (Switzerland)*, *14*(21). https://doi.org/10.3390/su142113903

Brasted, R. C. (2025). Tellurium Chemical element. *Earth Sciences.* Accessed on June 09, 2025 from https://www.britannica.com/science/tellurium

Brown, M. E. (2004). Reaction kinetics from thermal analysis. In *Introduction to Thermal Analysis* (pp. 181–214). Kluwer Academic Publishers. https://doi.org/https://doi.org/10.1007/0-306-48404-8_10

Cantor, B. (2020). The Avrami Equation: Phase Transformations. In *The Equations of Materials* (pp. 180–206). Oxford University Press. https://doi.org/https://doi.org/10.1093/oso/9780198851875.003.0009

Chemical Book. (2023). Tellurium dioxide: Tellurium dioxide Basic information. Accessed on June 07, 2025 from https://www.chemicalbook.com/ProductChemicalPropertiesCB1670143_EN.htm

Chivers, T., & Laitinen, R. S. (2015). Tellurium: A maverick among the chalcogens. *Chemical Society Reviews*, *44*(7), 1725–1739. https://doi.org/10.1039/c4cs00434e

Chung, H., Friedrich, S., Qu, M., & Friedrich, B. (2025). Hydrogen Reduction of Tellurium Oxide in a Rotary Kiln, Initial Approaches for a Sustainable Process. *Crystals*, *15*(5). https://doi.org/10.3390/cryst15050478

Dhyani, V., & Bhaskar, T. (2018). Kinetic analysis of biomass pyrolysis. In *Waste Biorefinery: Potential and Perspectives*. Elsevier B.V. https://doi.org/10.1016/B978-0-444-63992-9.00002-1

Ehlmé, E., Gunnarsson, A., Andersson, K., & Normann, F. (2023). Heat Transfer Conditions in Hydrogen-Fired Rotary Kilns for Iron Ore Processing. *Industrial and Engineering Chemistry Research*, *62*(37), 15098–15108. https://doi.org/10.1021/acs.iecr.3c02264

European Commission. (2021). Hydrogen As the Reducing Agent in the Recovery of metals and minerals from metallurgical waste. *CORDIS, HORIZON 2020*.

https://doi.org/https://doi.org/10.3030/958307

European Commission. (2023). The Adoption of Hydrogen Metallurgy in Climate-Neutral Production of Steel. *CORDIS, HORIZON EUROPE*. https://doi.org/https://doi.org/10.3030/101120068

Fedunik-Hofman, L., Bayon, A., & Donne, S. W. (2019). Kinetics of solid-gas reactions and their application to carbonate looping systems. *Energies*, *12*(15). https://doi.org/10.3390/en12152981

Friedrich, S. (2025). Process Technology of Metals: Thermal operations in non-ferrous metallurgy. *Supporting Documentation for lecture held at IME*, *RWTH Aachen University obtained on June 15, 2025.*

FTEL. (2023). Tellurium: the Unsung Hero of Sustainable Energy Innovation. Accessed on June 02, 2025 from https://firsttellurium.com/article/sustainable-energy-technologies-how-tellurium-is-driving-innovation/

Gaete-Argel, A., Velásquez, F., Márquez, C. L., Rojas-Araya, B., Bueno-Nieto, C., Marín-Rojas, J., Cuevas-Zúñiga, M., Soto-Rifo, R., & Valiente-Echeverría, F. (2021). Tellurite Promotes Stress Granules and Nuclear SG-Like Assembly in Response to Oxidative Stress and DNA Damage. *Frontiers in Cell and Developmental Biology*, *9*(February), 1–12. https://doi.org/10.3389/fcell.2021.622057

Gbor, P. K., & Jia, C. Q. (2004). Critical evaluation of coupling particle size distribution with the shrinking core model. *Chemical Engineering Science*, *59*, 1979–1987. https://doi.org/10.1016/j.ces.2004.01.047

Goldfarb, R. J., Berger, B. R., George, M. W., & Seal R. R. (2017). Tellurium, Chap. R. In *Critical mineral resources of the United States—Economic and environmental geology and prospects for future supply: U.S. Geological Survey Professional Paper 1802* (R1-R27, Vol. 1802). https://doi.org/https://doi.org/ 10.3133/pp1802R.

Haubner, R., Schubert, W. D., Hellmer, H., Lassner, E., & Lux, B. (1983). Mechanism of Technical Reduction of Tungsten: Part 2. Hydrogen Reduction of Tungsten Blue Oxide To Tungsten Powder. *International Journal of Refractory Metals and Hard Materials*, *2*(4), 156–163.

Ivanov, I. I., Shelemet'ev, V. M., Ul'yanov, V. V., & Teplyakov, Y. A. (2015). Kinetics of the Reduction of Orthorhombic and Tetragonal Lead Oxides to Lead with Hydrogen. *Kinetics and Catalysis*, *56*(3), 304–307. https://doi.org/10.1134/S0023158415030076

Jander, V. W. (1927). Reaktionen im festen Zustande bei hoheren Temperaturen. *163*(1), 1–30. https://doi.org/http://dx.doi.org/10.1002/zaac.19271630102

Khawam, A., & Flanagan, D. R. (2006). Solid-state kinetic models: Basics and mathematical fundamentals. *Journal of Physical Chemistry B*, *110*(35), 17315–17328. https://doi.org/10.1021/jp062746a

Kim, J. Y., Hanson, J. C., Frenkel, A. I., Lee, P. L., & Rodriguez, J. A. (2004). Reaction of CuO with hydrogen studied by using synchrotron-based x-ray diffraction. *Journal of Physics Condensed Matter*, *16*(33). https://doi.org/10.1088/0953-8984/16/33/008

King, P. L., Wheeler, V. W., Renggli, C. J., Palm, A. B., Wilson, S., Harrison, A. L., Morgan, B., Nekvasil, H., Troitzsch, U., Mernagh, T., Yue, L., Bayon, A., Difrancesco, N. J., Baile, R., & Kreider, P. (2018). Gas – Solid Reactions : Theory , Experiments and Case Studies Relevant to Earth and Planetary Processes. *Reviews in Mineralogy & Geochemistry*, *84*, 1–56.

Krauklis, A. E., & Dreyer, I. (2018). A Simplistic Preliminary Assessment of Ginstling-Brounstein Model for Solid Spherical Particles in the Context of a Diffusion-Controlled Synthesis. *Open Chemistry*, *16*(1), 64–72. https://doi.org/10.1515/chem-2018-0011

Lee, D. S., & Min, D. J. (2019). A Kinetics of Hydrogen Reduction of Nickel Oxide at Moderate Temperature. *Metals and Materials International*, *25*(4), 982–990. https://doi.org/10.1007/s12540-019-00261-y

Li, Z. (2020). General rate equation theory for gas–solid reaction kinetics and its application to CaO carbonation. *Chemical Engineering Science*, *227*, 115902. https://doi.org/10.1016/j.ces.2020.115902

Liu, C., Ding, X., Liu, H., Yan, X., Dong, C., & Wang, J. (2021). Numerical Analysis on Characteristics of Reduction Process within a Pre-Reduction Rotary Kiln. *Metals, 11*, 1180. https://doi.org/10.3390/met11081180

Luidold, S., & Antrekowitsch, H. (2007). Hydrogen as a Reducing Agent: Thermodynamic Possibilities. *Jom (Overview)*, 58–62.

Medina-Cruz, D., Tien-Street, W., Vernet-Crua, A., Zhang, B., Huang, X., Murali, A., Chen, J., Liu, Y., Garcia-Martin, J. M., Cholula-Díaz, J. L., & Webster, T. (2020). Tellurium, the Forgotten Element: A Review of the Properties, Processes, and Biomedical Applications of the Bulk and Nanoscale Metalloid. In B. Li, T. F. Moriarty, T. Webster, & M. Xing (Eds.), *Racing for the Surface: Antimicrobial and Interface Tissue Engineering* (pp. 723–783). Springer Nature. https://doi.org/10.1007/978-3-030-34471-9_15

Melchiori, T., & Canu, P. (2014). Improving the Quantitative Description of Reacting Porous Solids : Critical Analysis of the Shrinking Core Model by Comparison to the Generalized Grain Model. *Industrial and Engineering Chemistry Research 9*, 35131. Accessed on May 15, 2025 from https://pubs.acs.org/IECR

Miškovičová, Z., Legemza, J., Demeter, P., Buľko, B., Hubatka, S., Hrubovčáková, M., Futáš, P., & Findorák, R. (2024). An Overview Analysis of Current Research Status in Iron Oxides Reduction by Hydrogen. *Metals*, *14*(5). https://doi.org/10.3390/met14050589

Moss, R. L., Tzimas, E., Kara, H., Willis, P., & Kooroshy, J. (2011). Assessing Rare Metals as Supply-Chain Bottlenecks in Low-Carbon Energy Technologies. In *Eur 24884 En*. https://doi.org/10.2790/35600

Mungyeko Bisulandu, B. J. R., & Huchet, F. (2023). Rotary kiln process: An overview of physical mechanisms, models and applications. *Applied Thermal Engineering*, *221*. https://doi.org/10.1016/j.applthermaleng.2022.119637

National Center for Biotechnology Information. (2025). Compound Summary for CID 62638, Tellurium dioxide. *PubChem*. Accessed on June 10, 2025 from https://pubchem.ncbi.nlm.nih.gov/compound/Tellurium-dioxide.

Nomura, S. (2021). Low carbon ironmaking technologies: Japan's approach. *Iron Ore: Mineralogy, Processing and Environmental Sustainability*, 751–776. https://doi.org/10.1016/B978-0-12-820226-5.00022-7

Pale, P., & Mamane, V. (2023). Chalcogen Bonding Catalysis: Tellurium, the Last Frontier? *Chemistry - An European Journal*, *29*(69). https://doi.org/10.1002/chem.202302755

Papamichael, E. M., Stamatis, H., Stergiou, P. Y., Foukis, A., & Gkini, O. A. (2019). Enzyme Kinetics and Modeling of Enzymatic Systems. In *Advances in Enzyme Technology, First Edition*. Elsevier B.V. https://doi.org/10.1016/B978-0-444-64114-4.00003-0

Paunović, P., Načevski, G., Petrovski, A., Tomova, A., Grozdanov, A., & Dimitrov, A. T. (2019). Kinetic Analysis of Ultrasound Leaching of Nickel Laterite Ore. *Bulgarian Chemical Communications,* vol. 51, special issue D (pp.12 – 18)

Pei, M., Petäjäniemi, M., Regnell, A., & Wijk, O. (2020). Toward a Fossil Free Future With Hybrit: Development of Iron and Steelmaking Technology in Sweden and Finland. *Metals*, *10*(7), 1–11. https://doi.org/10.3390/met10070972

Provis, J. L. (2016). On the Use of the Jander Equation in Cement Hydration Modelling. *Rilem Technical Letters* 1: 62 – 66. https://doi.org/10.21809/rilemtechlett.2016.13

Quiñonez, E. (2025). Rotary kiln: operation, key models and industrial applications. *Inspenet.* Accessed on June 10, 2025 from https://inspenet.com/en/articulo/rotary-kiln-principle-and-applications/

Rombach, E., & Friedrich, B. (2014). Recycling of Rare Metals. *Handbook of Recycling: State-of-the-Art for Practitioners, Analysts, and Scientists*, 125–150. https://doi.org/10.1016/B978-0-12-396459-5.00010-6

RSC. (2025). Tellurium-Element information, properties and Uses. *Royal Society of Chemistry*. Accessed on June 03, 2025 from https://periodic table.rsc.org/element/52/tellurium#:~:text=Tellurium has been used to,or tin in semiconductor applications.&text=Tellurium has no known biological role.

Satoshi, T. (2019). Solid State Reactions and Sintering. In J. Hojo (Ed.), *Materials Chemistry of Ceramics* (pp. 45–74). Springer Nature Singapore Pte Ltd. https://doi.org/10.1007/978-981-13-9935-0

Schulmeyer, W. V., & Ortner, H. M. (2002). Mechanisms of the hydrogen reduction of molybdenum oxides. *International Journal of Refractory Metals and Hard Materials*, *20*(4), 261–269. https://doi.org/10.1016/S0263-4368(02)00029-X

Shirzad, K., & Viney, C. (2023). A critical review on applications of the Avrami equation beyond materials science. *Journal of the Royal Society Interface*, *20*(203). https://doi.org/10.1098/rsif.2023.0242

Sloman, B. M., Please, C. P., & Gorder, R. A. V. (2019). Homogenization of a Shrinking Core Model for Gas-Solid Reactions in Granular Particles. *Siam Journal of Applied Mathematics,* vol. *79*(1), 177–206. https://doi.org/10.1137/17M1159634.

Stewart, D. (2017). Tellurium Element Facts. *Chemicool Cooler than Absolute Zero!* Accessed on

June 17, 2025 from https://www.chemicool.com/elements/tellurium.html

Sun Furnace editorial team. (2025). Rotary kiln furnace – What is it? An easy-to-understand explanation of the structure, design, and applications by temperature. *Sun Furnace Co., Ltd., Design and Manufacture of Industrial Furnaces*. Accessed on June 20, 2025 from https://sunfa.co.jp/en/resources/column/column-2644/

Taheri, S. K. (1982). Direct Reduction of Iron Ore in a Rotary Kiln. *A thesis submitted for the degree of Doctor of Philosophy*. Brunel University (Department of Metallurgy), Great Britain.

Tang, J., Chu, M. sheng, Li, F., Feng, C., Liu, Z. gen, & Zhou, Y. sheng. (2020). Development and Progress on Hydrogen Metallurgy. *International Journal of Minerals, Metallurgy and Materials*, *27*(6), 713–723. https://doi.org/10.1007/s12613-020-2021-4

Tomić-Tucaković, B., Majstorović, D., Jelić, D., & Mentus, S. (2012). Thermogravimetric Study of the Kinetics of Co_3O_4 Reduction by Hydrogen. *Thermochimica Acta*, *541*, 15–24. https://doi.org/10.1016/j.tca.2012.04.018

Trawiński, B., & Kusz, B. (2021). Kinetic Analysis of the Reduction of a Ternary System of Bi, Sb and Te Oxides by Hydrogen for BiSbTe3 Synthesis. *Thermochimica Acta*, *701*(March). https://doi.org/10.1016/j.tca.2021.178966

Vijayan, S. N., & Sendhilkumar, S. (2014). Industrial Applications of Rotary Kiln in Various Sectors - A Review. *International Journal of Engineering Innovation & Research*, *3*(3), 342–345.

Vyazovkin, S., Burnham, A. K., Criado, J. M., Pérez-Maqueda, L. A., Popescu, C., & Sbirrazzuoli, N. (2011). ICTAC Kinetics Committee Recommendations for Performing Kinetic Computations on Thermal Analysis Data. *Thermochimica Acta*, *520*(1–2), 1–19. https://doi.org/10.1016/j.tca.2011.03.034

Wagner, D., Devisme, O., Patisson, F., & Ablitzer, D. (2008). A Laboratory Study of the Redution of Iron Oxide by Hydrogen. In F. Kongoli & R. G. Reddy (Eds.), *Sohn International Symposium* (Issue 2, pp. 111–120). Research Gate. https://www.researchgate.net/publication/1915819

Wei, Y., Yu, S., Guo, Q., Missen, O. P., & Xia, X. (2023). Microbial Mechanisms to Transform the Super-trace Element Tellurium: A Systematic Review and Discussion of Nanoparticulate Phases. *World Journal of Microbiology and Biotechnology*, *39*(10). https://doi.org/10.1007/s11274-023-03704-2

Zeng, Z., Kopasz, P. J., Krause, T., Yanguas-Gil, A., & Li, M. (2024). Direct Reduction of Iron by Hydrogen Plasma in a Rotary Kiln Reactor (US20240110254). Accessed on June 20, 2025 from https://labpartnering.org/patents/US20240110254

Zhang, X., Jiao, K., Zhang, J., & Guo, Z. (2021). A Review on Low Carbon Emissions Projects of Steel Industry in the World. *Journal of Cleaner Production*, *306*, 127259. https://doi.org/10.1016/j.jclepro.2021.127259

APPENDIX

APPENDIX A**: Summary of hydrogen reduction studies in rotary kiln**

Sources	Method	Highlights
Chung *et al.,* (2025)	Hydrogen gas in an oscillating kiln furnace at laboratory scale	Reduction up to 89 % achieved in solid gas
Taheri (1982)	Mixture of hydrogen-rich gas ($H_2/CO_2/C_4H_{10}$) in a rotary kiln at laboratory scale	Successful conversion of hematite iron ore to iron
Liu *et al.,* (2021)	Modelling, Mixture of hydrogen and carbon monoxide in pre-reduction rotary kiln	Metallization rate above 70 %
Zeng *et al.,* (2024)	Hydrogen gas and hydrogen plasma in rotary kiln	Efficiency in reduction and intensified kinetics

APPENDIX B: **Summary of projects representing advancement in hydrogen metallurgy**

Project	Country	Aims
HYBRIT	Sweden	Development of direct reduced iron and steel production technology with green hydrogen produced from renewable energy as a reducing agent.
COURSE50	Japan	Intensification of hydrogen reduction of iron ore and carbon dioxide capture through the utilization of waste heat in steel works targeted at 30 % reduction in carbon dioxide.
HELIOS	Austria, Belgium, Finland, Netherland	Provision of expertise in the field of hydrogen-based green steel production to doctoral candidates through collaborations with industries, universities and research centers.
HARARE	Belgium, Germany, Greece, Norway, Sweden	Application of hydrogen-based processes in the recovery of metallurgical waste from aluminium and copper production and to achieve environmentally friendly metal industry.
SALCOS	Germany	Production of green hydrogen from water splitting using electricity generated from wind and subsequently using the hydrogen as a reducing agent in steelmaking.

APPENDIX C: **Summary of research focused on hydrogen reduction**

Reference	Process	Conclusion
(Wagner et al., 2008)	Reduction of FeO_2 to Fe by hydrogen	A sequential reduction process as: $FeO_2 \rightarrow Fe_2O_3 \rightarrow FeO \rightarrow Fe$.
(Luidold & Antrekowitsch, 2007)	Overview of the possibility of hydrogen reduction of oxides, chlorides, sulfides and fluorides to produce metals.	Metals can be produced in solid (Powdery), liquid or gaseous forms at the reduction temperatures.
(Ivanov et al., 2015)	Reduction of PbO to Pb by hydrogen	Similar reactivity of oxides (tetragonal and orthorhombic) at temperature studied.
(Haubner et al., 1983)	Reduction of WO_3 to W by hydrogen	Process involved a transition as: $WO_{2.9x} \rightarrow WO_{2.9} \rightarrow WO_{2.72} \rightarrow WO_2 \rightarrow W$
(Schulmeyer & Ortner, 2002)	Reduction of MoO_3 to Mo	A two-step process: Step 1: $MoO_3 \rightarrow Mo_4O_{11} \rightarrow MoO_2$, Step 2: $MoO_2 \rightarrow Mo$.
(Lee & Min, 2019)	Reduction of NiO to Ni by hydrogen	Reduction behavior depends on both the temperature and particle size of oxide.
(Tomić-Tucaković et al., 2012)	Reduction of Co_3O_4 to Co by hydrogen	Two-step transformation revealed as: $Co_3O_4 \rightarrow CoO$ and $CoO \rightarrow Co$.
(Kim et al., 2004)	Reduction of CuO to Cu by hydrogen	A direct reduction at normal hydrogen flow and occurrence of a suboxide (Cu_2O) at very small hydrogen flow

		and heating rate above 20 ºC per minute.
(Trawiński & Kusz, 2021)	Reduction of mixture of Bi_2O_3, Sb_2O_3 and TeO_2 to $BiSbTe_3$ by hydrogen.	Complex mechanism as presence or absence of any of the oxides influence the overall reaction mechanism.

APPENDIX D: **Calculation of Theoretical Mass loss of Tellurium Oxide**

$$\text{mass loss}_{\text{theo}} = \frac{molar\ mass_{oxygen}}{molar\ mass_{tellurium\ oxide}} \times 100\%$$

Molar mass of oxygen = 16 g/mol. Molar mass of oxygen in tellurium oxide (TeO_2) = 16 + 16 = 32 g/mol. Molar mass of tellurium = 127.6 g/mol. Molar mass of tellurium oxide (TeO_2) = 127. 6 + 32 = 159.6 g/mol.

$$\text{mass loss}_{\text{theo}} = \frac{32}{159.6} \times 100\% \quad = 20.05013\ \%$$

Therefore, the theoretical mass loss used in the study is 20.05 %.